NAVAL POSTGRADUATE SCHOOL

MONTEREY, CALIFORNIA

THESIS

POTENTIAL VORTICITY ANALYSIS OF LOW LEVEL THUNDERSTORM DYNAMICS IN AN IDEALIZED SUPERCELL SIMULATION

by

Robert T. Davenport

March 2009

Thesis Advisor:	Wendell A. Nuss
Second Reader:	Karl D. Pfeiffer

Approved for public release; distribution is unlimited

THIS PAGE INTENTIONALLY LEFT BLANK

REPORT DOCUMENTATION PAGE			Form Approved OMB No. 0704-0188
Public reporting burden for this collection of information is estimated to average 1 hour per response, including the time for reviewing instruction, searching existing data sources, gathering and maintaining the data needed, and completing and reviewing the collection of information. Send comments regarding this burden estimate or any other aspect of this collection of information, including suggestions for reducing this burden, to Washington headquarters Services, Directorate for Information Operations and Reports, 1215 Jefferson Davis Highway, Suite 1204, Arlington, VA 22202-4302, and to the Office of Management and Budget, Paperwork Reduction Project (0704-0188) Washington DC 20503.			
1. AGENCY USE ONLY ***(Leave blank)***	**2. REPORT DATE** March 2009	**3. REPORT TYPE AND DATES COVERED** Master's Thesis	
4. TITLE AND SUBTITLE Potential Vorticity Analysis of Low Level Thunderstorm Dynamics in an Idealized Supercell Simulation			**5. FUNDING NUMBERS**
6. AUTHOR(S) Robert T. Davenport			
7. PERFORMING ORGANIZATION NAME(S) AND ADDRESS(ES) Naval Postgraduate School Monterey, CA 93943-5000			**8. PERFORMING ORGANIZATION REPORT NUMBER**
9. SPONSORING /MONITORING AGENCY NAME(S) AND ADDRESS(ES) N/A			**10. SPONSORING/MONITORING AGENCY REPORT NUMBER**
11. SUPPLEMENTARY NOTES The views expressed in this thesis are those of the author and do not reflect the official policy or position of the Department of Defense or the U.S. Government.			
12a. DISTRIBUTION / AVAILABILITY STATEMENT Approved for public release; distribution is unlimited			**12b. DISTRIBUTION CODE**

13. ABSTRACT (maximum 200 words)

Potential vorticity "thinking" has been used to infer the balanced dynamics of predominately synoptic-scale weather features. This is accomplished through the use of the invertibility principle in which the wind and mass fields can be retrieved from the three-dimensional distribution of potential vorticity (PV). The most common use of PV thinking has been applied to various forms of synoptic-scale cyclogenesis and the sensitivity of certain weather features had on the subsequent development.

Utilizing the non-linear balance PV inversion developed by Davis and Emanuel (1991) this study extends the current use of PV diagnostics to atmospheric features and motions on the order of the meso- and storm-scale. This study, in essence becomes a feasibility study to examine whether a primarily synoptic-scale diagnostic tool can be applied to much smaller scales and inherently more complex fields of motion that occur within a supercell thunderstorm. An idealized supercell simulation from the ARW will be used to examine the low level thunderstorm dynamics from a PV perspective.

The results show promise that the PV diagnostic can be applied to thunderstorm dynamics given the qualitative results presented here. Refinements are necessary to improve the quantitative accuracy of this technique.

14. SUBJECT TERMS Potential Vorticity, Severe Weather, Supercell, Weather Research and Forecasting Model, Advanced WRF			**15. NUMBER OF PAGES** 65
			16. PRICE CODE
17. SECURITY CLASSIFICATION OF REPORT Unclassified	**18. SECURITY CLASSIFICATION OF THIS PAGE** Unclassified	**19. SECURITY CLASSIFICATION OF ABSTRACT** Unclassified	**20. LIMITATION OF ABSTRACT** UU

NSN 7540-01-280-5500 Standard Form 298 (Rev. 2-89)
Prescribed by ANSI Std. 239-18

THIS PAGE INTENTIONALLY LEFT BLANK

Approved for public release; distribution is unlimited

POTENTIAL VORTICITY ANALYSIS OF LOW LEVEL THUNDERSTORM DYNAMICS IN AN IDEALIZED SUPERCELL SIMULATION

Robert T. Davenport
Captain, United States Air Force
B.S., University of Oklahoma, 2004

Submitted in partial fulfillment of the
requirements for the degree of

MASTER OF SCIENCE IN METEOROLOGY

from the

NAVAL POSTGRADUATE SCHOOL
March 2009

Author: Robert T. Davenport

Approved by: Wendell A. Nuss
Thesis Advisor

Karl D. Pfeiffer
Second Reader

Philip A. Durkee
Chairman, Department of Meteorology

THIS PAGE INTENTIONALLY LEFT BLANK

ABSTRACT

Potential vorticity “thinking” has been used to infer the balanced dynamics of predominately synoptic-scale weather features. This is accomplished through the use of the invertibility principle in which the wind and mass fields can be retrieved from the three-dimensional distribution of potential vorticity (PV). The most common use of PV thinking has been applied to various forms of synoptic-scale cyclogenesis and the sensitivity of certain weather features had on the subsequent development.

Utilizing the non-linear balance PV inversion developed by Davis and Emanuel (1991) this study extends the current use of PV diagnostics to atmospheric features and motions on the order of the meso- and storm-scale. This study, in essence becomes a feasibility study to examine whether a primarily synoptic-scale diagnostic tool can be applied to much smaller scales and inherently more complex fields of motion that occur within a supercell thunderstorm. An idealized supercell simulation from the ARW will be used to examine the low level thunderstorm dynamics from a PV perspective.

The results show promise that the PV diagnostic can be applied to thunderstorm dynamics given the qualitative results presented here. Refinements are necessary to improve the quantitative accuracy of this technique.

THIS PAGE INTENTIONALLY LEFT BLANK

TABLE OF CONTENTS

THIS PAGE INTENTIONALLY LEFT BLANK

LIST OF FIGURES

LIST OF TABLES

THIS PAGE INTENTIONALLY LEFT BLANK

ACKNOWLEDGMENTS

I would first like to thank my thesis advisor, Prof Nuss, and second reader, Lt Col. Pfeiffer. Prof Nuss' tireless efforts in developing a working potential vorticity inversion code and subsequent guidance was the key factor in producing the results presented in this thesis. I am also grateful for the numerical modeling assistance provided by Lt Col. Pfeiffer and my constant troubleshooting requests that kept him busy throughout the research process. I also need to thank Mr. Bob Creasey for his computer help and timely efforts in gathering much need meteorological data and Mr. Albert Barreto for setting up the virtual machine to run the numerical weather model.

I would finally like to thank my family for all the support and understanding they have provided during my time here at school. For my wife, Elizabeth, and the birth of our baby girl, Kayleigh; it was truly an amazing and blessing experience. And for my son, Michael, whose constant requests to play trains and trucks provided ample opportunity for me to watch him grow and experience the world though his eyes.

THIS PAGE INTENTIONALLY LEFT BLANK

I. INTRODUCTION

Thunderstorm forecasting has and will continue to be a primary concern for meteorologists due to the varied nature of convection and the weather hazards these storms produce. Storms can produce a variety of weather phenomena that could be considered severe (Johns and Doswell 1992) and represent a significant hazard to the public (Brooks et al. 1994a). The most commonly recognized threats being heavy rain, large hail, damaging winds, and tornadoes. Forecasters frequently use pattern recognition as a primary tool to forecast favorable environmental conditions related to the development of severe convective storms. The fundamental components necessary for severe convection are (i) sufficient low level moisture, (ii) conditional instability and (iii) a trigger, or mechanism to lift warm, moist low level air to its level of free convection (LFC) (Doswell 1987, Johns and Doswell 1992). A fourth condition, vertical shear of the horizontal winds, helps determine the convective mode after thunderstorm initiation has begun (Gold and Nielsen-Gammon 2008a, part one of four part series, hereafter GNG1).

While questions remain about the link between the synoptic-scale environment and the mode and intensity of convection, it has been relatively agreed upon that the synoptic-scale environment creates conditions favorable for severe weather (GNG1, Johnson and Mapes 2001). Forecasters usually expect an increase in severe weather probabilities in the presence of an upper level trough. However, there is still continued difficulty in determining the most common type of severe weather that will occur even when forecasters correctly anticipate a severe weather outbreak (Johns and Hart 1993, GNG1). Forecasters diagnose environmental regions supportive of severe weather but the importance of synoptic-scale flow and subsynoptic-scale processes is still difficult to determine (Doswell 1987, GNG1). This inherent difficulty in forecasting severe weather arises from the multitude of mesoscale processes that work to initiate convection.

Johnson and Mapes (2001) describe the mesoscale processes that work to (i) precondition the environment, (ii) initiate convection, and (iii) provide convective feedback to the environment. The convectively generated cold pool is a mesoscale feature that can act in each of the three ways. It is then logical to assume that the cold

pool plays an important role in thunderstorm dynamics. The cold pool forms when evaporatively cooled air in the downdraft reaches the ground and spreads out horizontally (Engerer et al. 2008). Recent attention by Engerer et al. (2008) has been given to the study of surface characteristics of colds pools from mesoscale convective systems (MCS) using the Oklahoma Mesonet (see Brock et al. 1995 for a description). The results found by Engerer et al. (2008) showed a substantial drop in potential temperature with the passage of the gust front that represents the leading edge of the cold pool. This temperature deficient could allow the cold pool to be characterized as a negative PV anomaly.

The concept of PV invertibility has made it possible to retrieve the wind and mass fields from a given distribution of PV based on an appropriately chosen balance constraint (e.g. Hoskins et al. 1985 hereafter HMR85, Bluestein 1993). This technique has been successfully applied to studies on extra- and tropical cyclogenesis (e.g. Davis and Emanuel 1991, hereafter DE91, Davis et al. 1996, Huo et al. 1999) and more recently, has been applied to the severe convective environment (e.g. Roebber et al. 1999, Gold and Nielsen-Gammon four part series 2008) to diagnose mid tropospheric shortwave troughs. These studies have used PV inversion to both quantify and qualitatively describe the sensitivity a certain upper level feature has on a particular weather event. Hoskins et al. (1985) and Thorpe (1985) showed that atmospheric PV anomalies have a surface equivalent, namely, potential temperature anomalies.

The nonlinear balance (NLB) PV inversion developed by DE91 and supercell simulations from the Weather Research and Forecasting (WRF) model version three will be used in this study. While most PV studies are most commonly applied to synoptic-scale processes, this study hopes to extend the current use of PV diagnostics toward mesoscale processes since it is those processes that play a major role in initiating convection. The cold pool is an important mesoscale feature for the development of convection and simultaneously be represented as a surface temperature anomaly. The edge of the cold pool is also important as horizontal vorticity is tilted into the vertical and ingested into the thunderstorm's updraft. This study becomes, in essence, a feasibility

exercise to examine whether PV inversion can be applied to mesoscale and even storm-scale processes with a focus on low level features that affect convective development.

The remaining sections of the thesis is organized as follows; background information, data and methodology, data and results and finally conclusions and future research. The Background (Chapter II) contains information on the (i) WRF model and Advanced Research WRF supercell simulation, (ii) potential vorticity, and (iii) convective dynamics and characteristics of cold pools. Chapter III describes the supercell simulation and the potential vorticity inversion technique. The data and results (Chapter IV) is divided into three parts based on the convective lifecycle; (i) early development, (ii) storm splitting, and (iii) supercell development. Chapter V provides the conclusions and areas of future research

THIS PAGE INTENTIONALLY LEFT BLANK

II. BACKGROUND

A. THE ADVANCED RESEARCH WRF

The WRF model is a numerical weather prediction model that contains two different systems designed to support operational and research applications (Skamarock et al. 2008). The operational subset is the WRF-NMM (Non-hydrostatic Mesoscale Model) and is used to produce the standard, daily operational weather forecasts. The other subset is the WRF-ARW (Advanced Research WRF) and is used to support a wide range of research applications. The ARW is designed to handle real-data and idealized forecasts and simulations due to its large variety of physical and dynamical options. Use of the WRF preprocessing system (WPS) is required for real-data studies. The WPS is a set of programs that take meteorological and terrestrial data and transforms them into a format suitable for input into the ARW. An overview of WRF system components is given in Figure 1.

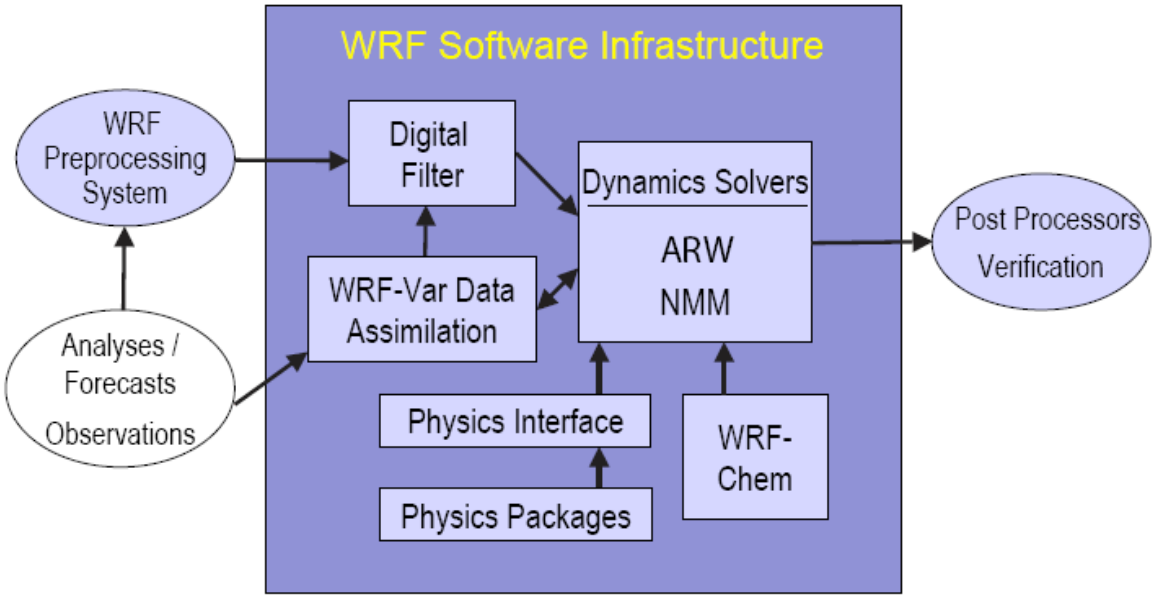

Figure 1. WRF system components. From Skamarock et al. (2008).

The ARW is composed of the ARW dynamics solver and the other compatible components of the WRF system (e.g., physics packages, numeric and dynamic options, data assimilation). The latest version, 3, was released in April 2008. All the information presented on the ARW has been taken directly from the National Center for Atmospheric Research (NCAR) Technical note NCAR/TN-475+STR (Skamarock et al. 2008) and the online WRF modeling systems user guide (Wang et al. 2008) located at http://www.mmm.ucar.edu/wrf/users/docs/user_guide_V3/. The reader is referred to these sources for additional technical information not presented here. Some additional references are also provided on specific features of the ARW model where more information can be obtained.

The ARW dynamics solver integrates the compressible, non-hydrostatic, Euler equations in flux form (see Ooyama 1990). The equations used a terrain-following hydrostatic-pressure vertical coordinate (Laprise 1992) commonly referred to as eta-levels.

The ARW is discretized over time and space. Temporal discretization is performed through a time-split integration scheme described by Wicker and Skamarock (2002). This approach prevents the meteorologically insignificant (high-frequency) modes from limiting the time step of the third-order Runge-Kutta (RK3) scheme used to integrate the slower, meteorologically significant modes. Spatial discretization uses the Arakawa C grid staggering. That is, velocities are staggered one-half grid length from the thermodynamic variables as shown in Figure 2.

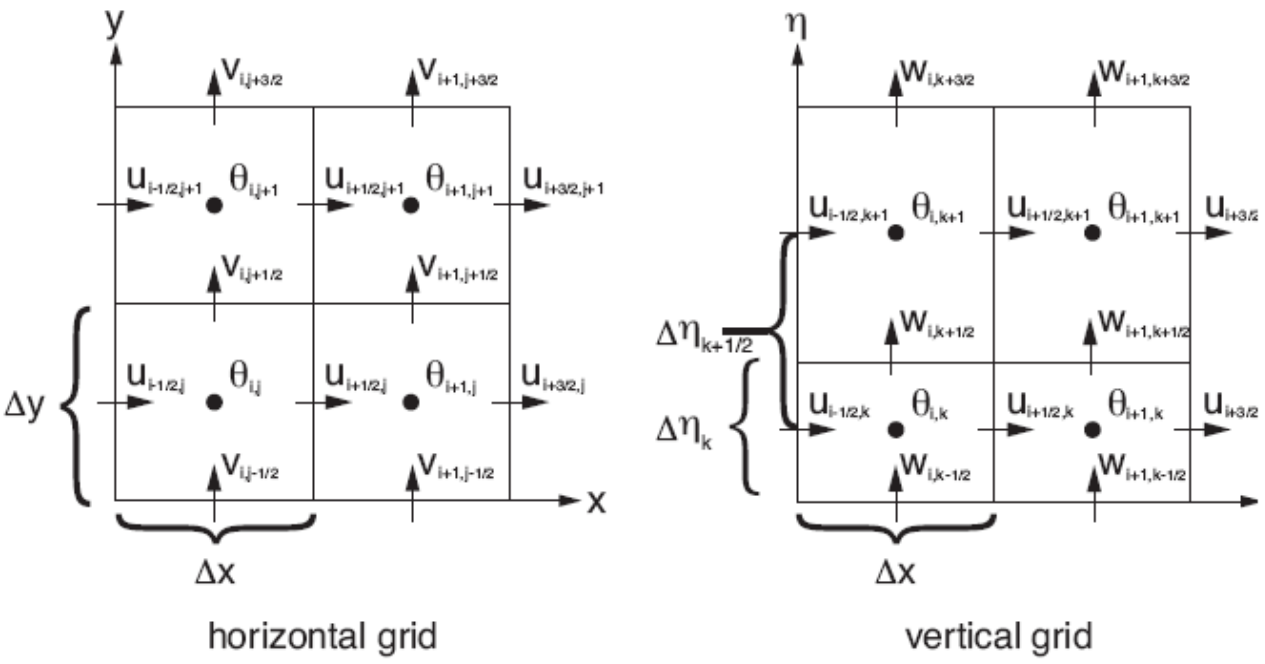

Figure 2. Horizontal and vertical grids for the ARW. From Skamarock et al. (2008).

The ARW model physics have many options available. The five main categories are (i) microphysics, (ii) cumulus parameterizations, (iii) planetary boundary layer (PBL), (iv) land-surface model (LSM), and (v) radiation. Each of these five categories contains many specific parameterizations to choose from. There are also many interactions (Table 1) between the parameterizations and the state variables and their tendencies. Physics drivers separate the physics section from the dynamic solvers. The physics drivers are divided between a pre-physics preparation step and post-physics modification of variable tendencies.

Table 1. Physics Interactions. Columns correspond to model physical processes: radiation (Rad), microphysics (MP), cumulus parameterization (CP), planetary boundary layer/vertical diffusion (PBL), and surface physics (Sfc). Rows correspond to model variables where i and o indicate whether a variable is input or output (updated) by a physical process. From Skamarock et al. (2008)

		Rad	MP	CP	PBL	Sfc
Atmospheric State or Tendencies	Momentum			i	io	
	Pot. Temp	io	io	io	io	
	Water Vapor	io	io	io	io	
	Cloud	io	io	o	io	
	Precip	io	io	o		
Surface Fluxes	Longwave Up	i				o
	Longwave Down	o				i
	Shortwave Up	i				o
	Shortwave Down	o				i
	Sfc Convective Rain			o		i
	Sfc Resolved Rain		o			i
	Heat Flux				i	o
	Moisture Flux				i	o
	Surface Stress				i	o

B POTENTIAL VORTICITY

1. Overview and the Invertibility Principle

The simplest form of PV is based on the work of Rossby (1940) and Ertel (1942). Describing the two dominant processes in the vorticity budget, vorticity is created by vertical stretching of vortex tubes and by the horizontal advection of absolute vorticity. The overall concept of potential vorticity asserts that there is a potential for creating vorticity by changing the latitude of the parcel and by adiabatically altering the distance that separates the layer bounded by two isentropic surfaces (HMR85). Thus, PV can be thought of as a measure of the ratio of absolute vorticity to the effective depth of the layer containing the vortex (Holton 1992). Rossby (1940) and then Ertel (1942) expressed this relationship as

$$PV = -g(f + \hat{k} \cdot \nabla_\theta \times \hat{v}) \frac{\partial \theta}{\partial p} \tag{1}$$

where $\zeta_\theta = \hat{k} \cdot \nabla_\theta \times \hat{v}$, is the isentropic vorticity, $\hat{k}$ is the vertical unit vector and ∇_θ is the three dimensional gradient operator in x, y, θ space (HMR85). This relationship showed that isentropic PV, or Ertel PV, is conserved in an adiabatic, frictionless atmosphere and for balanced flow or unbalanced flow (HMR85, DE91, Bluestein 1993, Morgan and Nielsen-Gammon 1998, hereafter MGN98).

Early work using PV mainly focused on its significance as an air-mass tracer. Kleinschmidt, through a series of papers in the 1950's, pushed the use of PV and tried to explain cyclogenesis using upper tropospheric PV anomalies (HMR85). This work led to the formulation known today as the "invertibility principle" for PV, namely that one can diagnose the complete atmospheric flow structure from the spatial distribution of PV (Kleinschmidt 1950a, b, 1951, HMR85, Bluestein 1993). The ability to invert the PV field and retrieve the wind and mass fields allows PV to become a useful diagnostic tool for the dynamical processes that occur in the atmosphere.

The application of the invertibility principle requires additional information in order to obtain the individual fields of absolute vorticity and static stability. To perform the inversion, the (i) reference state of the atmosphere must be specified, (ii) an appropriate balance condition must be imposed, and (iii) the inversion must be solved globally with proper boundary conditions (HMR85). The use of a proper reference state, balance condition (e.g. geostrophy, gradient wind balance, non-linear balance) and boundary conditions allows us to find the exact combination of absolute vorticity and static stability associated with the global PV field (HMR85, Bluestein 1993).

2. Distribution of PV in the Atmosphere

Recall Rossby's form of potential vorticity in Eq (1) where PV is the product of the isentropic vorticity and static stability. The standard PV can be simplified to

$$PV \approx -gf \frac{\partial \theta}{\partial p}. \tag{2}$$

Substituting typical values associated with mid latitude synoptic scale flow into Eq (2):

$$PV = -(10\ m\,s^{-2})(10^{-4}\ s^{-2})\left(-\frac{10\,K}{10\ kPA}\right)\frac{1\ kPa}{10^3\ kg\,m\,s^{-2}\,m^{-2}} \tag{3}$$

$$= 10^{-6}\ m^2\ s^{-1}\ K\ kg^{-1} = 1\ PVU \quad (4)$$

where a PVU is a potential vorticity unit. PV values approximately less than 1.5 PVU are usually associated with tropospheric air while higher values are associated with stratospheric air (Bluestein 1993).

This boundary between tropospheric and stratospheric PV can be characterized by the dynamic tropopause. The dynamic tropopause is defined based on a constant value of PV instead of the standard lapse rate definition (MNG98). Various values of PV have been used to define the tropopause but the most commonly used values range from 1-3 PV units. This range usually lies in the transition region between the upper troposphere and lower stratosphere. Due to different thermal stratification and different concentrations of certain chemical constituents (e.g., ozone induced stratospheric warming); the stratosphere tends to have higher values of PV than the upper troposphere (MNG98, Gerard 1998). At high latitudes, this region of high PV values is often referred to as the stratospheric reservoir. Equatorward protrusions of relative PV maxima indicate regions where stratospheric air is descending into the troposphere. Figure 3 shows the average vertical distribution of Ertel's PV for July. As expected, the tropopause is highest over the tropics and slopes downward over the poles. The stratospheric reservoir is also easily recognized over the higher latitudes and poles.

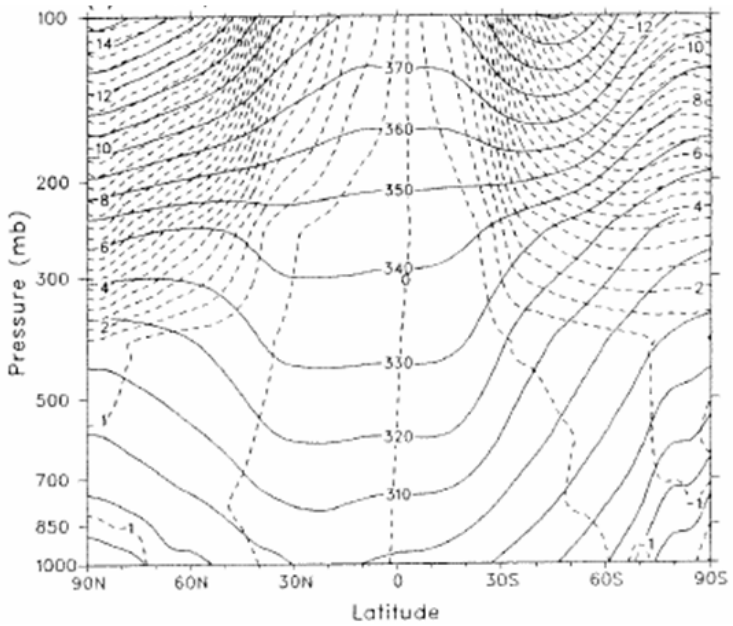

Figure 3. Vertical cross section of zonal mean of Ertel's potential vorticity in PVU (dashed lines) and potential temperature in K (solid lines) for July; from 1979-1989 initialized ECMWF data at seven levels, twice daily. From Bluestein (1993).

3. Atmospheric PV Anomalies

The invertibility principle uses the idea that the atmosphere can be described as the summation of all positive and negative PV anomalies and the wind field is a summation of the individual wind fields attributable from each separate anomaly (Bluestein 1993). A correlation should then be made that relates the PV field to a more commonly used meteorological field. Figure 4 shows the time evolution from 12 UTC 11 March 2006 to 12 UTC 12 March 2006 using the 11/12Z GFS model run. Relative maxima PV values correspond to cyclonic curvature and cooler air associated with troughs and closed lows.

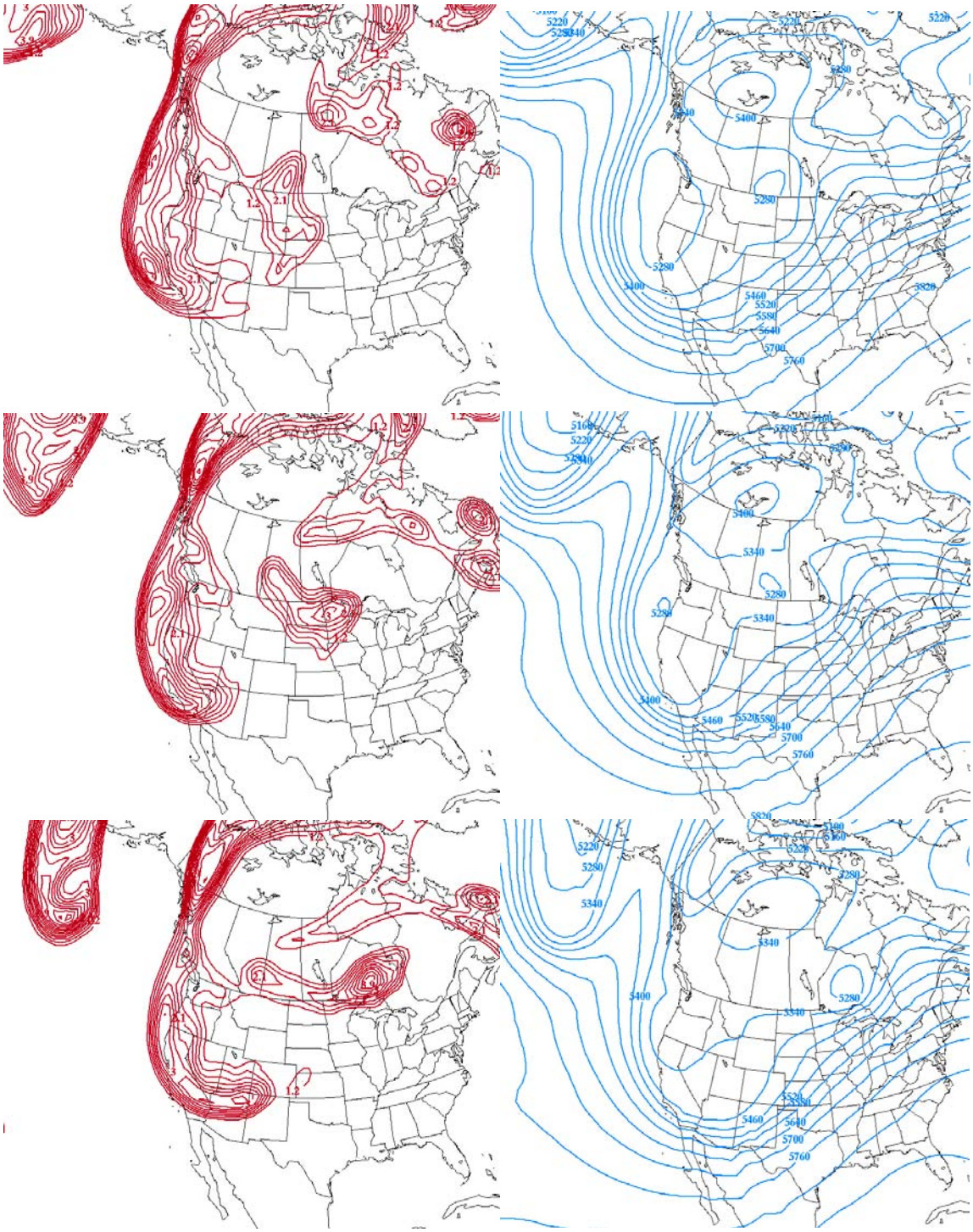

Figure 4. Potential vorticity (left) and corresponding 500 mb height field in meters (right) from the 12 UTC 03/11/2006 GFS model run. Top row: 11/12Z initialization. Middle row: 12 hour forecast valid at 12/00Z. Bottom row: 24 hour forecast valid at 12/12Z. Only positive PVU values greater than 1 PVU are shown.

While only positive PVU values are shown, the same inference can be drawn from relative minima PV values. PV minima correspond to anticyclonic curvature and warmer air associated with ridges and blocking cyclones. Thus, one can define relative maxima (minima) PV values as positive (negative) PV anomalies (HMR85, Bluestein 1993). A note must be made that the positive (negative) term refers to the Northern Hemisphere only. To be precise, a positive (negative) PV anomaly should be classified as cyclonic (anticyclonic) which holds true for the Southern Hemisphere. Since our case study is focused in the United States, positive and negative terms will used.

We define PV as the product of absolute vorticity and static stability (Eq 1). A positive PV anomaly would then be more stable than a negative PV anomaly assuming absolute vorticity being equal for both anomalies. Given this difference in static stability, a positive PV anomaly would see the isentropes in a vertical cross section bend toward the center of the anomaly. This would increase the static stability of the anomaly itself while decrease the stability above and below the anomaly due to a weakening of the potential temperature gradient. Figures 5 and 6 show the vertical cross sections of a positive and negative PV anomaly respectively.

Thorpe (1985) used the non-linear polar coordinate form of the PV equation

$$\frac{\partial}{\partial r}\left(\frac{1}{r}\frac{\partial(rV)}{\partial r}\right)+\frac{\zeta_{a\theta}}{\sigma^{*}}\frac{1}{g}\frac{\partial}{\partial\theta}\left(\frac{f_{loc}}{K(p)}\frac{\partial V}{\partial\theta}\right)+\frac{\partial f}{\partial r}=\sigma^{*}\frac{\partial P}{\partial r} \tag{5}$$

to solve for idealized, circularly symmetric positive and negative PV anomalies where:

$$K(p)=\frac{\partial}{\partial p}\left[C_p\left(\frac{p}{p_0}\right)^{R/C_p}\right] \tag{6}$$

$$f_{loc}=f+\frac{2V}{r}. \tag{7}$$

The parameter f_{loc} is the absolute local rotation rate where f is from the Earth's rotation and $2V/r$ is the relative rotation around the origin. V is the wind speed, $\zeta_{a\theta}$ is the absolute vorticity on an isentropic surface, and σ^{*} is a measure of the static stability (Bluestein 1993). The full derivation of Eq (5) can be found in Bluestein (1993). The schematic results of Thorpe's (1985) solutions are depicted in Figure 7a for a positive PV

anomaly and Figure 7b for a negative PV anomaly. For more detail on the computational method used, see Thorpe (1985) and Bluestein (1993). The observed structures of atmospheric anomalies are accurately depicted in Thorpe's (1985) solutions by comparing Figures 5 and 6 with Figure 7.

The positive PV anomaly is characterized by a relative high static stability and surrounded by a cyclonic circulation. The static stability above the positive anomaly is relative low. The negative PV anomaly is characterized with a relative low in static stability and an anticyclonic circulation. The atmosphere has high static stabilities above and below the negative anomaly.

Bluestein (1993) and HMR85 used Thorpe's (1985) results to show that vorticity and static stability are positively correlated with PV anomalies on isentropic surfaces. This is also the true for individual anomalies of vorticity and static stability. Thermal wind balance suggests that a positive PV anomaly caused by vorticity alone would cause the isentropes to squeeze together toward the center of the anomaly thus increasing static stability. The same reasoning also holds for a PV anomaly composed entirely of a static stability anomaly. Radial pressure on the isentropes would have to correspond to an increase in vertical shear and thus vorticity around the anomaly (Bluestein 1993).

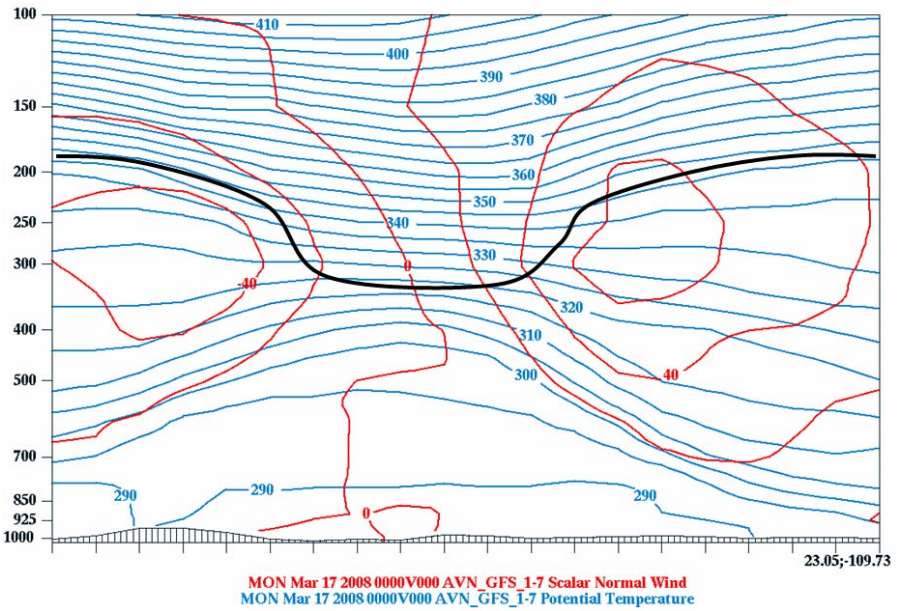

Figure 5. Vertical cross section through an upper level positive PV anomaly at 00 UTC, March 17, 2008. Cross section taken along a north-northwest to south-southeast line from San Francisco, Ca to Cabo San Lucas, MEX. Potential temperature in K (blue contours); scalar normal winds (red contours). Tropopause is indicated by thick, black line.

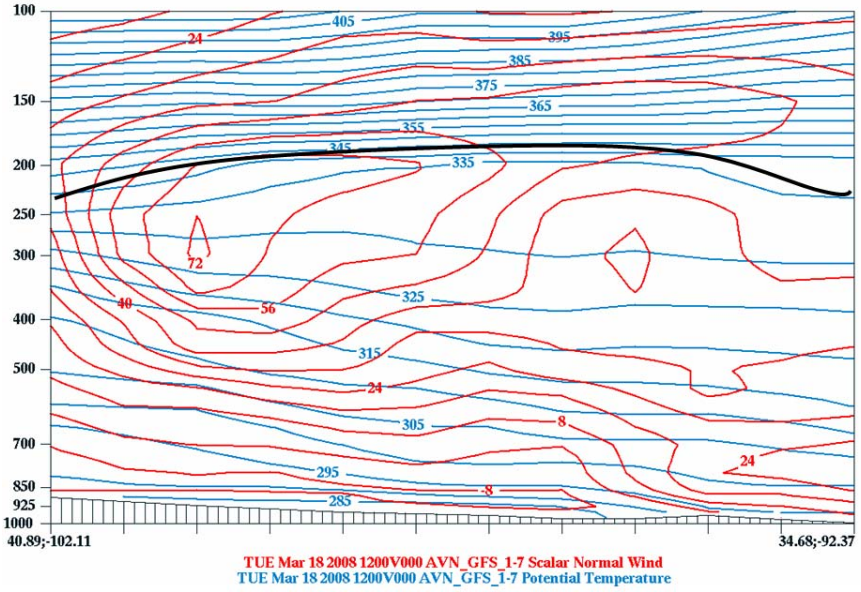

Figure 6. As in Figure 5 but for a vertical cross section through an upper level negative PV anomaly at 12 UTC, March 18, 2008. Cross section taken along a northwest to southeast line from North Platte, NE to Little Rock, AR.

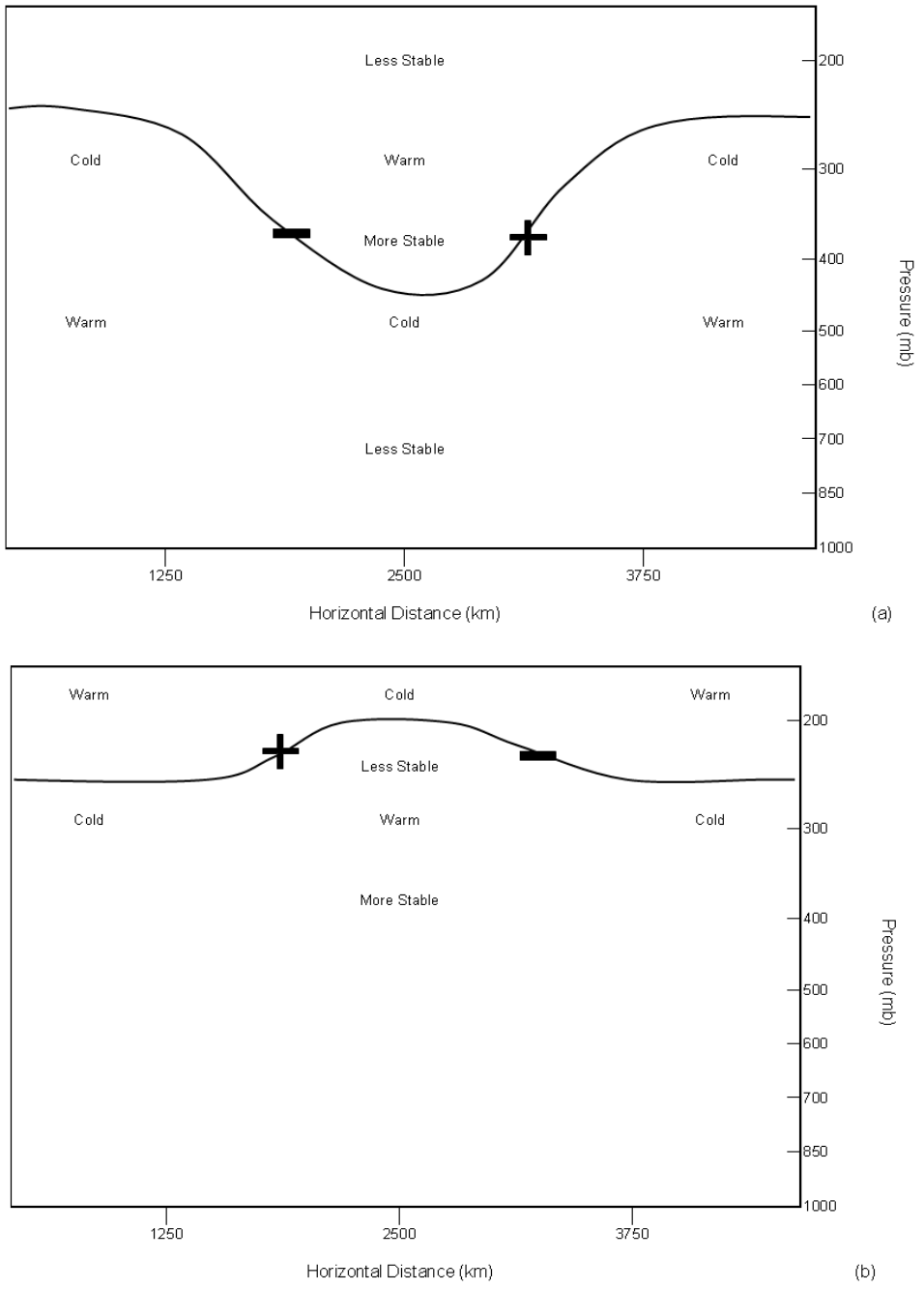

Figure 7. The cross sectional view of the schematic results from Thorpe's solutions to Eq (2.5) for a (a) positive PV anomaly and (b) negative PV anomaly. Tropopause (thick solid line); center of anomaly located at 2500 km near the tropopause; the + and – indicate the location of maximum normal wind flow into and out of the cross section plane, respectively. From Bluestein (1993)

4. Surface Potential Temperature Anomalies

Solutions for Eq (5) were also computed by Thorpe (1985) for idealized, circularly symmetric anomalies in surface potential temperature with no upper level PV anomaly present. Schematic results are shown in Figure 8.

As with atmospheric PV anomalies, a correlation can be seen between warm and cold surface potential temperature anomalies with vorticity and static stability. A warm surface anomaly has higher static stability as isentropes bend downward toward the anomaly and bunch at the surface. Assuming an unperturbed upper level flow, the warm core anomaly must induce a cyclonic vortex based on anticyclonic thermal wind shear present. This same reasoning can also be applied to a cold surface potential temperature anomaly. However, the cold anomaly is not confined to the surface but extends upward like a cold dome. This is due to the weakened static stability as the isentropes bend upward away from the anomaly. An anticyclonic circulation occurs around the cold anomaly due to cyclonic thermal wind shear (Thorpe 1985, HMR85, Bluestein 1993).

Based on the results from Thorpe (1985), a warm (positive) potential temperature anomaly at the surface is equivalent to a positive PV anomaly and a cold (negative) potential temperature anomaly is equivalent to a negative PV anomaly.

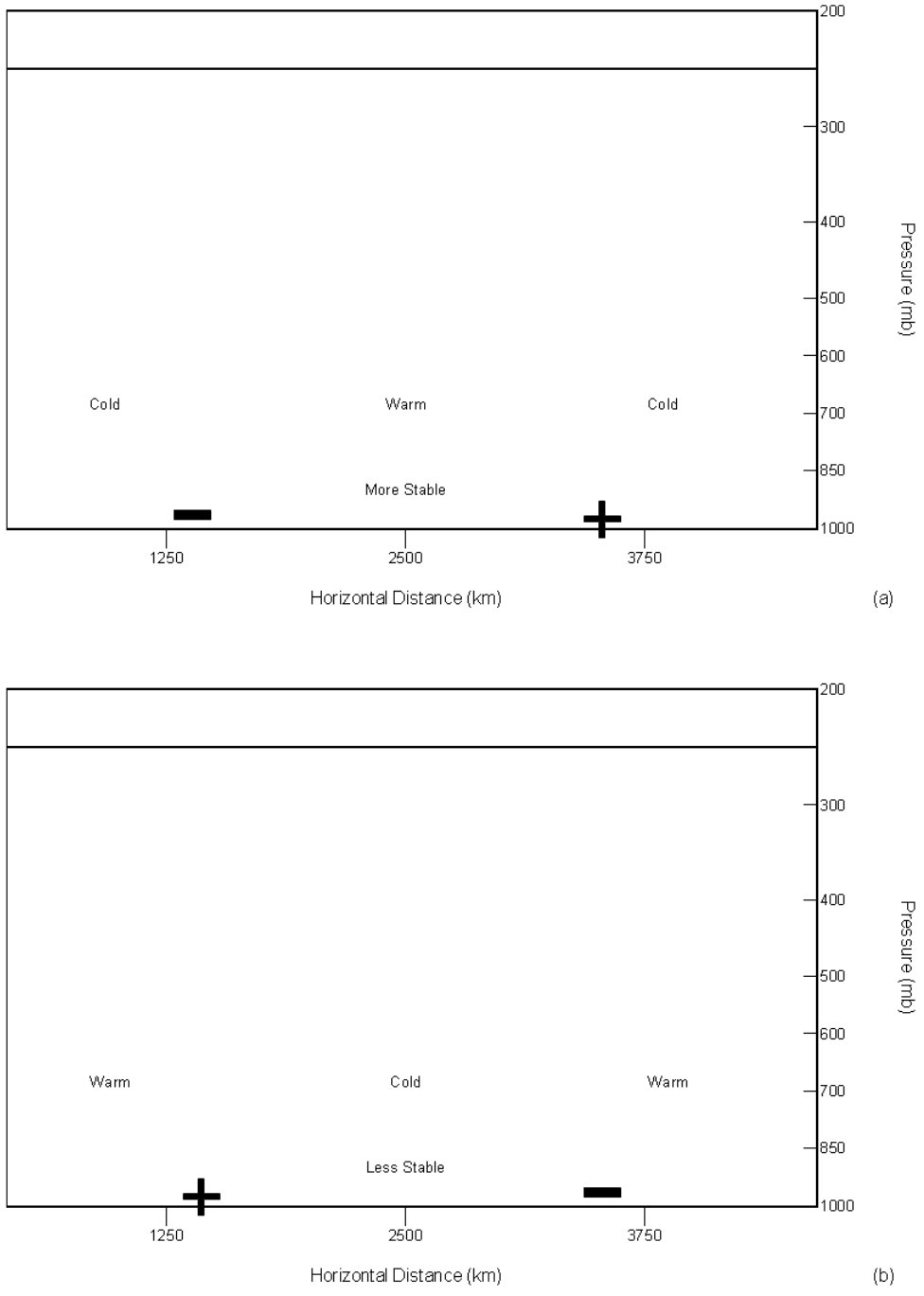

Figure 8. The cross sectional view of the schematic results from Thorpe's solutions to Eq (2.5) for a (a) warm surface potential temperature anomaly and (b) cold potential temperature anomaly. Tropopause (thick solid line); center of anomaly located at 2500 km near the ground; the + and – indicate the location of maximum normal wind flow into and out of the cross section plane, respectively. From Bluestein (1993)

5. PV Influences on the Severe Environment

The sensitivity of atmospheric variables can be examined with the use of PV invertibility. Previous studies (e.g. Dickinson et al. 1997, Huo et al. 1999, Roebber et al. 2002) have used a concept called PV surgery to understand how a specific PV anomaly affected a particular weather event. PV surgery involves removing a specific PV anomaly and inverting the remaining PV field to quantify the effects of the anomaly in question. In order to use PV invertibility to diagnose severe convective weather, the convective parameters must be linked to the balanced and unbalanced wind and height fields (GNG1).

Storm-relative environmental helicity (SREH), vertical shear (SHR), bulk Richardson number shear (BRNSHR) and convective available potential energy (CAPE) are some of the most common parameters associated with severe convection. These parameters can be calculated once the wind and height fields have been retrieved from the PV inversion (GNG1) as shown below:

$$SREH = \int_{sfc}^{z} \left(\vec{V} - \vec{C}\right) \cdot \nabla \times \vec{V}\, dz = \int_{sfc}^{z} \hat{k} \times \frac{d\vec{V}}{dz} \cdot \left(\vec{V} - \vec{C}\right) dz \tag{8}$$

$$SRH = \left\| \vec{V}_6 - \vec{V}_{PBL} \right\| \tag{9}$$

$$BRNSHR = 0.5 \times \left(\bar{u}^2 + \bar{v}^2\right) \tag{10}$$

$$CAPE = \int_{\ln p_{LNB}}^{\ln p_0} R_d \left(T_{v_{par}} - T_v\right) d \ln p = \int_{p_{LNB}}^{p_0} R_d \left(\frac{T_{v_{par}} - T_v}{p}\right) dp \tag{11}$$

where z is the assumed flow depth, $\bar{C}$ is the storm motion vector calculated using the method derived by Bunkers et al. (2000). V_6 is the 6 km wind, V_{PBL} is the wind in the planetary boundary layer (PBL), and $\bar{u}$ and $\bar{v}$ are the component differences between the mass weighted winds in the 0-6 km layer and the PBL. The equation for CAPE consists of the parcel's virtual temperature, $T_{v_{par}}$, the parcel's original level, p_0, and the parcel's level of neutral buoyancy, p_{LNB} (Brooks et al. 1994a, GNG1). Operational forecasters

use these parameters to quantify the buoyancy and wind shear which are then used to determine the mode, intensity, and longevity of thunderstorms (Weisman and Klemp, 1982).

Nielsen-Gammon and Gold (2008, part two of four part series, hereafter NGG2) demonstrated the effects of upper level PV changes on the convective parameters using a positive idealized, circularly symmetric PV anomaly. As seen in Figure 9, the results were consistent with those of Thorpe (1985) with the anomaly decreasing in magnitude as the horizontal and vertical distance increase. Applying these results to the severe convective environment, the downward bending of isentropes above the anomaly shows a warming of that layer. Conversely, the upward bending of the isentropes below the positive PV anomaly corresponded to a cooling of the atmosphere since potential temperature increases with height. This thermal structure is similar to the cold-core trough described by Thorpe (1986) and suggests that the region beneath and near the anomaly has a higher convective instability (GNG1).

Studies done by Jukes and Smith (2000) and MNG98 showed that CAPE is increased and convective inhibition is decreased directly under and near the positive PV anomaly. This change in the convective environment is due to lower values of potential temperature being pulled upward toward the anomaly causing a cooling in that section of the atmospheric column. Also seen in Figure 9 is an increase in the cyclonic circulation with height below the anomaly. This increase in winds with respect to height would increase the vertical shear below and near the anomaly and aid in developing an environment conducive for rotating updrafts (NGG2).

The amplification of the PV anomaly would intensify the effects listed above as the temperature perturbations increase above and below the anomaly. The atmospheric column below and near the intensified anomaly would experience an increase in the upward bending of the isentropes thus increasing the cooling. The cooling below the anomaly would act in the same manner as cold air advection and decrease the lapse rates in the mid levels of the atmosphere. This would increase CAPE and decrease CIN in the column beneath and near the anomaly and increase the probability of deep moist convection. The cyclonic circulation around the PV anomaly would also strengthen in

response to the amplification of the anomaly. This would likely lead to an increase of vertical shear in the convective environment. Large scale assent would also be affected as air flows up and along the isentropes. The upward bending of the isentropic surfaces would increase vertical motion beneath and downstream of the anomaly. Rising air would cool adiabatically and further cool the layer beneath the anomaly and add to the increased CAPE and decreased CIN (NGG2).

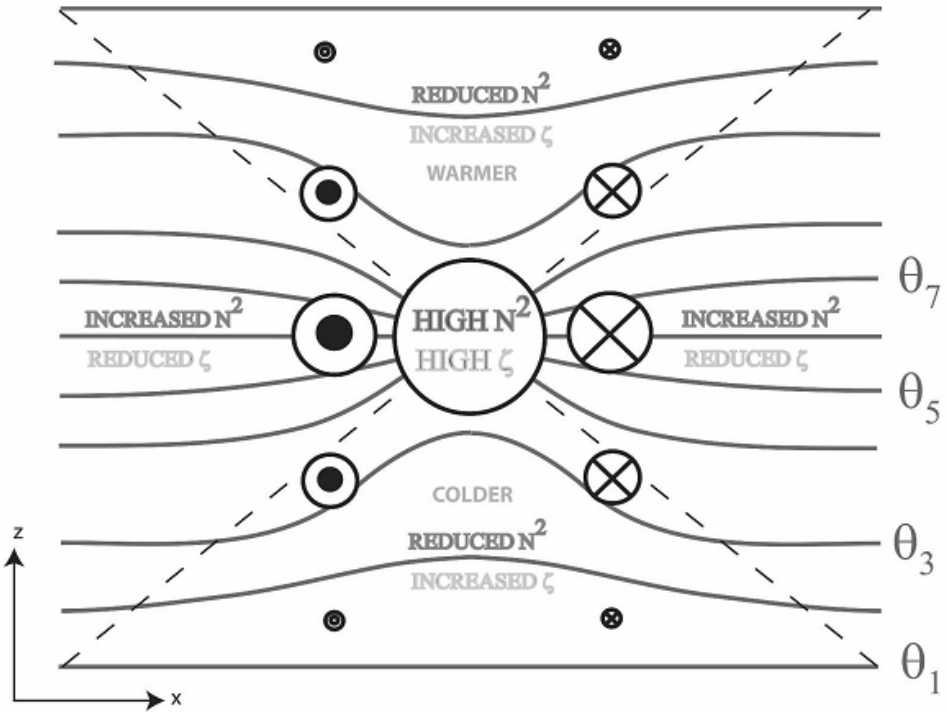

Figure 9. Idealized schematic of an isolated positive (cyclonic) spherical PV anomaly. Background state is uniform and the vertical axis is scaled by N_0/f_0. From NGG2.

C. CONVECTIVE DYNAMICS OF SEVERE THUNDERSTORMS

1. Overview

The first conceptual model of a thunderstorm was derived from data collected over Florida during the Thunderstorm Project. This project took place in the post World War II years as a joint venture between the Weather Bureau, National Advisory

Committee for Aeronautics ,U.S. Air Force and U.S. Navy to investigate the dynamics of thunderstorms (Byers and Braham 1948, Doswell 2001). While the conceptual model produced by Byers and Braham (1948) has changed with time and continuing research, the concept of the "thunderstorm cell" remains today as the basic organizational structure for convection (Doswell 2001), namely the formation of a single updraft and downdraft pair.

Numerous studies have detailed the severe convective environment and the structure of supercell thunderstorms. The need to accurately predict the formation of and subsequent motion of supercells has provided 50 plus years of research into the topic. The continued research on severe thunderstorms has also been guided by the fact that most supercells produce some type of severe weather (e.g. tornadoes, large hail, damaging winds or flashfloods) at some point during the life cycle of the storm (Burgess and Lemon 1991, Bunkers et al. 2000).

Following the terminology presented by Moller et al (1994) and Bunkers et al (2000), a supercell is defined as a convective storm that contains a mesocyclone or antimesocyclone with (i) the absolute value of vertical vorticity greater than or equal to 10^{-2} s^{-1}, (ii) persist at a minimum on the order of tens of minutes, and (iii) persist through at least one third of the storms depth. Right and left movers are classified by the direction they move relative to the vertical shear. Right (left) movers are mesocyclones (antimesocyclones) that travel to the right (left) of the vertical wind shear.

The dynamics of the severe thunderstorm environment: how thunderstorms develop and progress through their convective life cycles, has been well documented (e.g., Lemon and Doswell 1979, Weisman and Klemp 1982, Rotunno and Klemp 1985, Moller et al. 1994) along with the characteristic differences between tornadic and nontornadic storms (e.g., Brooks et al. 1994a, 1994b). Since the goal of this paper is to analyze the formation of rotating updrafts from a PV perspective, the focus should be placed on those environmental conditions and dynamics that create mesocyclones.

2. The Role of the Cold Pool in Convection

As already noted previously, the cold pool can affect the convective environment in multiple ways (Johnson and Mapes 2001). Byers and Braham (1948) and Newton and Newton (1959) noted that the cold pool was instrumental in the formation of new convection along the gust front or outflow boundary. The airmass discontinuity represented by the gust front acts in much the same way as a cold front. In some cases, conditionally unstable environmental air is lifted to its LFC along the gust front to form new convective cells. This is the primary process for the sustenance of multicell thunderstorms (Weisman and Klemp 1986, Engerer et al. 2008). Johnson and Mapes (2001) also describe the way cold pools precondition the environment. In these cases forced lifting of conditionally unstable air is unable to initiate convection by itself. The development of new convection then requires additional forcing. This can occur as the cold pool intersects other low level boundaries (e.g., other outflows, terrain, larger-scale fronts) to produce sufficient lift for convection. Purdom (1976) showed using satellite data from the Geostationary Operational Environment Satellite (GOES) that intersecting boundaries are often a focus for the intensification of convection. On larger scales, multiple cold pools can merge to cover hundreds of square kilometers and help to generate new convection hundreds of miles from the origin point of the cold pool (Engerer et al. 2008). The larger and stronger the difference between the cold pool and nearby environment, the longer such contrast can exist and spark new convection hours after the initial convection has ended (Doswell 2001, Johnson and Mapes 2001).

The cold pool is also an important feature for the generation of deep, moist convection (Rotunno et al. 1988) especially when combined with vertical shear of the environmental winds (Szeto and Cho 1994). Not only does the outflow boundary act to trigger new convective cells to sustain the propagation of squall lines and other types of MCSs, but increased vertical shear and convergence along the gust increases chances of severe weather (Maddox et al. 1980). Studies by Maddox et al. (1980) and Markowski et al. (1998) showed that pre-existing cold pools can lead to the development of strong tornadoes with the passage of supercells over the cold pool (Engerer et al. 2008). On the smaller, convective scales, cold pools generated by the forward-flank and rear-flank

downdrafts (FFD and RFD respectively) have been thought to play an important part in tornadogenesis. Brooks et al. (1994b) state that the occurrence of tornados in supercells is closely linked to the formation of a low level mesocyclone created from baroclinically generated vorticity in the evaporatively cooled downdrafts (Rotunno and Klemp 1985, Davies-Jones and Brooks 1993).

While cold pools have been intimately linked to the convective life cycle, a balancing act must occur between the cold pool and surrounding environment to promote continued convection. Thorpe et al. (1982) proposed that favorable conditions for strong, long-lived convection occurred when low level shear of the environment was sufficiently strong to prevent the cold pool from moving away from the cell (Rotunno et al. 1988). Otherwise, the cold pool could propagate away from the cell and cut off the warm, moist environmental air feeding the convective updraft and causing the thunderstorm to decay (Engerer et al. 2008).

3. Characteristics of Cold Pools

The cold pool originates inside the downdraft as evaporatively cooled air reaches the ground and spreads out along the surface. The accumulation of this cooler air creates a hydrostatic increase in surface pressure that is a function of temperature and cold pool depth (Wakimoto 1982, Engerer 2008). This area of higher pressure is commonly referred to as a mesohigh (Engerer 2008).

Bryan et al. (2005) measured the intensity of MCS generated cold pools in the stratiform precipitation regions from soundings taken during the Bow Echo and MCV Experiment (BAMEX). Bryan et al. (2005) measured cold pool intensity by C derived from the deep anelastic equations:

$$C^2 = -\frac{2}{\bar{\rho}(z=0)}\int_0^H (\bar{\rho}B)dz, \tag{12}$$

where z is the height, H is the cold pool depth, ρ is the density, and B is the buoyancy (neglecting hydrometeors):

$$B = g\left(\frac{\theta-\bar{\theta}}{\bar{\theta}} + 0.61(q_v - \bar{q}_v)\right). \tag{13}$$

In Eq (13), g is the gravitational acceleration, θ is the potential temperature, and q_v is the water vapor mixing ratio. The approximate height of the cold pool was calculated to be the height above ground where the buoyancy first reached $0\,m\,s^{-2}$. Over-bars indicate variables obtained from the environment conditions with other variables calculated from inside the cold pool.

The cold pools studied during BAMEX by Bryan et al. (2005) showed that most of the cold pools were deep and intense, with heights greater than three kilometers and values of C greater than $20\,m\,s^{-2}$. The authors noted that results of cold pool strength and intensity from the BAMEX study are different than values obtained from numerical studies. Bryan et al. (2005) argue that the results are an accurate representation of the environments during BAMEX and that the discrepancies likely resulted from these environmental differences.

Engerer et al. (2008) used the Oklahoma Mesonet to identify surface characteristics the MCS cold pools for four MCS life-cycle stages, (i) first storms, (ii) MCS initiation, (iii) mature MCS, and (iv) MCS dissipation. Engerer et al. (2008) found that average surface pressure rises from all stages was around 3 hPa. They also noted that the average potential temperature deficits inside the cold pool ranged from 9.8 to 5.6 K colder with the strongest deficit occurring during the first storms stage and decreasing an average of 1 K through each successive stage. Engerer et al. (2008) did observe a mean potential temperature deficit of nearly 11 K during the daytime and early evening observations. Using the low level potential temperature deficit associated with cold pools and the baroclinic generation of vorticity along the gust front, this study hopes to exploit the application of PV inversion to examine the feasibility of using this dynamical technique on smaller-scale features.

4. Thunderstorm Dynamics

The ability to determine convective storm types has typically relied on the use of buoyancy, usually measured by CAPE, and the vertical wind shear (Moller et al. 1994). These two parameters have been shown to be useful in discriminating between supercell

and non-supercell storm environments but not necessarily between tornadic and nontornadic storms (Brooks et al 1993, Brooks et al. 1994b). Droegemeier et al. (1993), with the use of numerically generated storms, showed that the storm-relative environmental helicity (Eq 8) was an indicator of the correlation between vertical velocity and vorticity. Higher helicity environments are then assumed to have a greater likelihood of supporting rotating updrafts.

A numerical modeling study by Weisman and Klemp (1982) showed that low level vertical shear in an unstable (positive CAPE) environment was the origin of midlevel rotation. This conclusion was also supported by theoretical studies done by Davies-Jones (1984) and Rotunno and Klemp (1985). Davies-Jones (1984) explained rotating updraft formation using streamwise vorticity. Convection deforms isentropic surfaces, which causes a tilting of the vortex tubes that lie along the isentropic surface. Rotunno and Klemp (1985) showed that the origin of mid-level updraft rotation was from the horizontal vorticity from environmental shear. The reader is referred to these two papers for more detailed information. Brooks et al. (1994b) state, however, that the occurrence of tornados in supercells is closely linked to the formation of a low level mesocyclone created from baroclinically generated vorticity in the evaporatively cooled downdrafts (Rotunno and Klemp 1985, Davies-Jones and Brooks 1993).

While different mechanisms are responsible for the rotation found to occur in thunderstorms, they all have a common trait. These mechanisms, to a high degree, are not controlled by the large-scale environment but by smaller-scale processes. Using the definitions of large-scale and mesoscale provided by Doswell (1987), large-scale features are those that can be described by quasi-geostrophic processes and mesoscale features are those that can be described only by considering the interactions of both large-scale and microscale processes. The evolution of synoptic scale features often creates an environment favorable for severe weather (e.g. low level moisture and conditional instability). However, large-scale lifting based on the quasi-geostrophic omega equation is insufficient to lift a parcel in its LFC on time scales necessary to initiate deep, moist convection thus it is the mesoscale interactions that affect the occurrence of convection (Doswell 1987). Consequently, the goal of this paper is to examine low level thunderstorm dynamics from a PV perspective in an effort to test whether PV inversion can be applied to smaller, more complex atmospheric motions.

III. DATA AND METHODOLOGY

A. ADVANCED RESEARCH WRF MODEL

1. Data, Model Setup, and Methodology

Data for this analysis will be obtained using the idealized supercell simulation from version three of the ARW. The domain will use the Cartesian coordinate system with a grid box 160 km x 160 km in both horizontal directions and 20 km in the vertical. Horizontal grid spacing is two kilometers and vertical grid spacing is 500 meters. The simulation will be run through three hours with a 12 second time step and WRF output data written at every five minute forecast time intervals.

The supercell will utilize the Purdue Lin microphysics scheme. This scheme contains six hydrometeor classes: water vapor, rain, snow, cloud ice, cloud water, and graupel or hail. No cumulus scheme is used with the two kilometer grid spacing (Dudhia 2006) allowing for the explicit cumulus development with resolved updrafts. The default settings for the supercell simulation neglect both the longwave and shortwave radiation schemes and the surface- and boundary-layer schemes. These default settings will be kept in order to simplify the simulation. The Coriolis terms in the model are turned off due to the short (three hour) time period of the simulation.

The supercell simulation will be run under ideal conditions using the default input sounding. The supercell simulation requires an input sounding that contains any set of levels up to the model top. The first line of the input sounding contains surface data, the surface pressure (hPa), potential temperature (K), and moisture mixing ratio (g/kg). Data for the input sounding contains the height above the surface (in meters), the potential temperature (K), vapor mixing ratio (g/kg) and the u and v wind components. The model then interprets and extrapolates (if necessary) the data before starting the simulation. The environmental winds of the input sounding produce a quarter circle hodograph. Both left and right moving supercells are produced with this input sounding. Figure 10 shows the sounding used to initialize the supercell simulation.

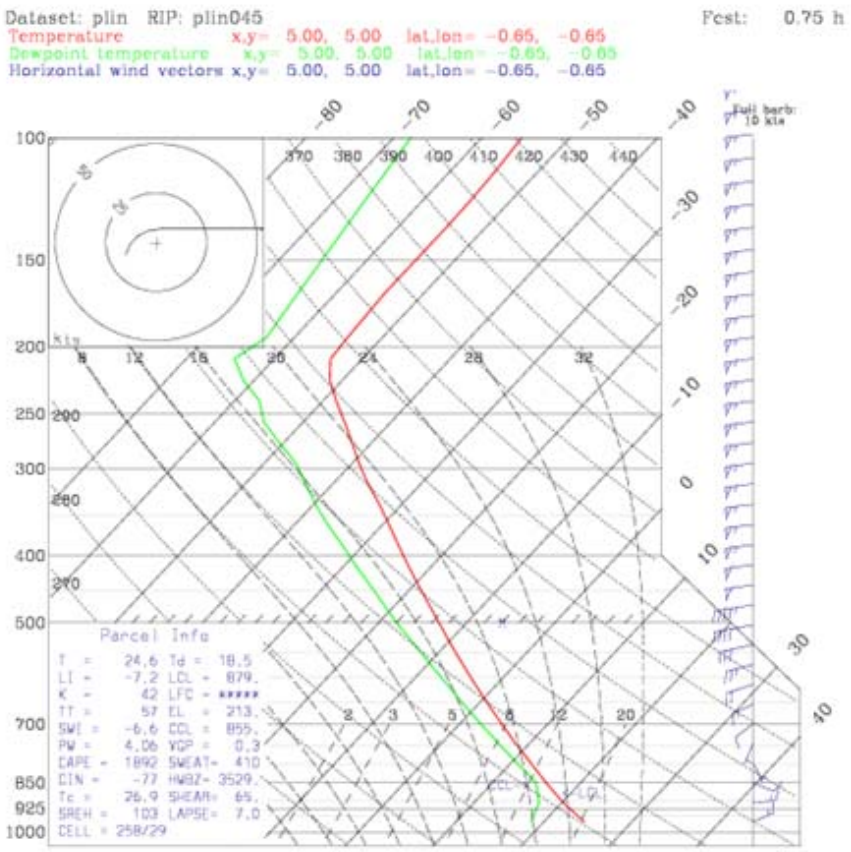

Figure 10. Input sounding used to initialize the supercell simulation

Using the concepts developed by Thorpe (1985) and HMR85 and focusing on the low level thunderstorm structure and dynamics, PV inversion will be used to see if the inverted wind and mass fields resemble the observed characteristics of thunderstorms.

2. PV Inversion Technique

The ability to invert the PV field requires the use of a balance system to relate the wind and mass fields to the distribution of PV. The balance system contains a balance equation that relates the streamfunction to the geopotential, a vorticity equation, thermodynamic equation and mass conservation equation (MNG98). Since the convective environment is highly ageostrophic in nature, a high order balance constraint must be used in order to accurately retrieve the wind and mass fields from the distribution

of PV. Specifically, DE91 developed a method for PV inversion using the nonlinear balance condition devised by Charney (1955) for Ertel PV.

While PV diagnostics using the nonlinear balance system have focused mainly on synoptic scale cyclogenesis, the NLB inversion should be applicable over a large range of atmospheric conditions (Nielsen-Gammon and Gold 2008a, hereafter NGGa). The PV framework provided by DE91 makes use of the NLB system in which the irrotational component of the horizontal wind field is small and can be neglected. This creates a small difference between the NLB PV and the hydrostatic Ertel PV (NGGa). For a given distribution of Ertel's PV, the NLB PV inversion of DE91 returns the following balanced variables; geopotential height and nondivergent streamfunction (DE91, GNG1). The reader is encouraged to consult DE91 for more information on the inversion technique.

The PV inversion technique used here follows that of DE91. The NLB (Ψ, Φ) and potential vorticity (q) equations are defined as

$$\nabla^2\Phi = \nabla f \nabla\Psi + f\nabla^2\Psi + 2\left(\frac{\partial^2\Psi}{\partial x^2}\frac{\partial^2\Psi}{\partial y^2} - \left(\frac{\partial^2\Psi}{\partial x \partial y}\right)^2\right) \tag{12}$$

and

$$q = \frac{gk\Pi}{p}\left(\left(f + \nabla^2\Psi\right)\frac{\partial^2\Psi}{\partial\Pi^2} - \frac{\partial^2\Psi}{\partial\Pi\partial x}\frac{\partial^2\Phi}{\partial\Pi\partial x} - \frac{\partial^2\Psi}{\partial\Pi\partial y}\frac{\partial^2\Phi}{\partial\Pi\partial y}\right) \tag{13}$$

with Π as the Exner function. The equations are both scaled by appropriate factors and the following equations used to formulate the PV inversion system become:

$$\frac{\nabla^2\Phi}{f} = \frac{\nabla f \nabla\Psi}{f} + \nabla^2\Psi + \frac{2}{f}\left(\frac{\partial^2\Psi}{\partial x^2}\frac{\partial^2\Psi}{\partial y^2} - \left(\frac{\partial^2\Psi}{\partial x \partial y}\right)^2\right) \tag{14}$$

$$\frac{p \cdot q}{gk\Pi} = \left(f + \nabla^2\Psi\right)\frac{\partial^2\Phi}{\partial\Pi^2} - \frac{\partial^2\Psi}{\partial\Pi\partial x}\frac{\partial^2\Phi}{\partial\Pi\partial x} - \frac{\partial^2\Psi}{\partial\Pi\partial y}\frac{\partial^2\Phi}{\partial\Pi\partial y} \tag{15}$$

The mass and wind fields are linked to the spatial distribution of PV by subtracting Eq (14) and Eq (15) and by adding Eq (14) and Eq (15). The two equations used to solve the PV inversion process are

$$\frac{\nabla^2\Phi}{f}+\left(f+\nabla^2\Psi\right)\frac{\partial^2\Phi}{\partial\Pi^2}=\frac{\nabla f\nabla\Psi}{f}+\nabla^2\Psi+\frac{2}{f}\left(\frac{\partial^2\Psi}{\partial x^2}\frac{\partial^2\Psi}{\partial y^2}-\left(\frac{\partial^2\Psi}{\partial x\partial y}\right)^2\right)+\frac{p\cdot q}{gk\Pi}+\frac{\partial^2\Psi}{\partial\Pi\partial x}\frac{\partial^2\Phi}{\partial\Pi\partial x}+\frac{\partial^2\Psi}{\partial\Pi\partial y}\frac{\partial^2\Phi}{\partial\Pi\partial y} \tag{16}$$

$$\left(f+\frac{\partial^2\Phi}{\partial\Pi^2}\right)\nabla^2\Psi=\frac{p\cdot q}{gk\Pi}+\frac{\partial^2\Psi}{\partial\Pi\partial x}\frac{\partial^2\Phi}{\partial\Pi\partial x}+\frac{\partial^2\Psi}{\partial\Pi\partial y}\frac{\partial^2\Phi}{\partial\Pi\partial y}+\nabla^2\Phi-\nabla f\nabla\Psi-2\left(\frac{\partial^2\Psi}{\partial x^2}\frac{\partial^2\Psi}{\partial y^2}-\left(\frac{\partial^2\Psi}{\partial x\partial y\partial}\right)^2\right) \tag{17}$$

where the geopotential height and streamfunction fields are solved for based on the distribution of PV. The solution uses a successive overrelaxation method following DE91. The PV field used in the calculations is derived from the model forecasted wind field and thermodynamic structure. PV inversion is then used to calculate the following variables: (i) u and v wind components, (ii) potential temperature, (iii) geopotential height, and (iv) streamfunction and streamlines.

IV. DATA ANALYSIS AND RESULTS

A. EARLY INITIATION

The thermal bubble used to initiate convection is located at the center of the domain. It is a two degree Kelvin temperature difference with a horizontal radius of 10 kilometers and 1500 meter vertical extent that forces a parcel to its LFC. Model derived radar echoes are first recorded around 15 minutes into the simulation associated with a towering cumulus cloud. Mean seal level pressure and 950 mb winds are plotted in Figure 11 along with streamlines.

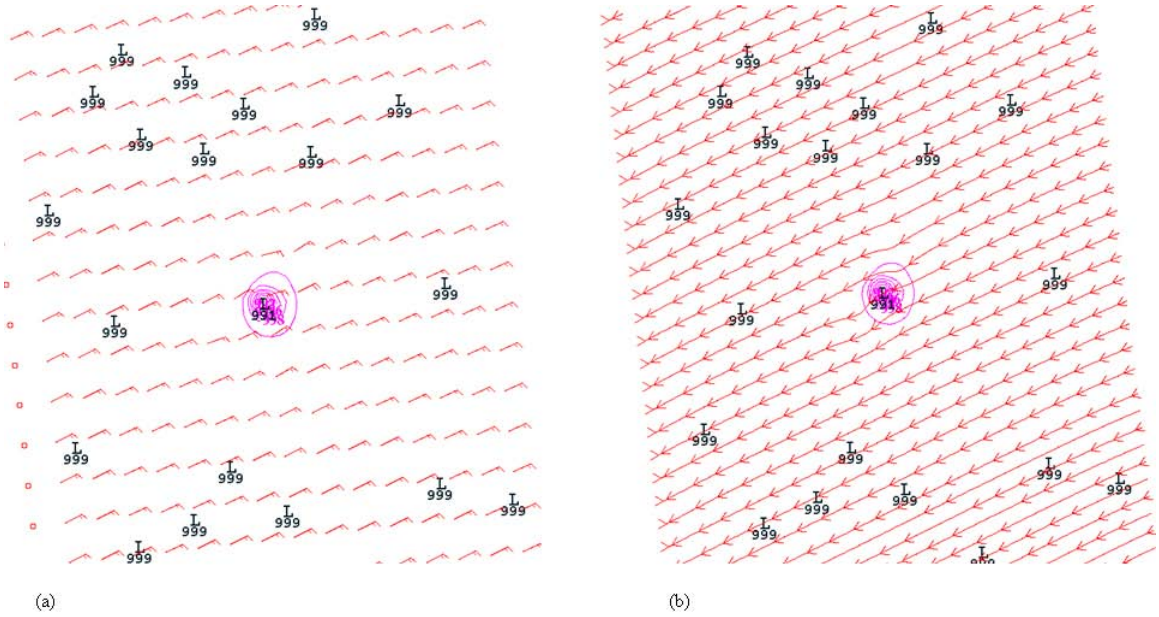

Figure 11. Plot of mean sea level pressure (purple) and the PV calculated 950 mb winds in (a) and 950 mb streamlines in (b) at 15 minutes into the simulation.

Developing convection is represented by the low pressure in the center of the domain that corresponds to the location of the thermal perturbation. As the rising column of air cools and condenses into a towering cumulus cloud (Figure 12), the PV derived wind field begins to show a low level cyclonic perturbation around the forming updraft.

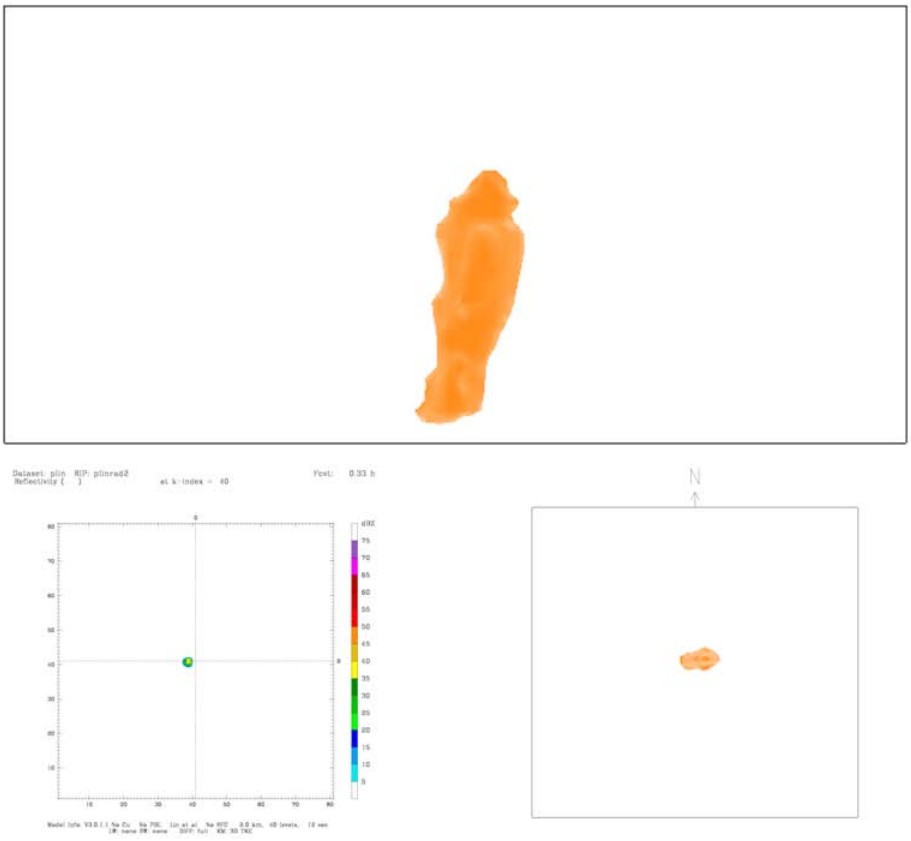

Figure 12. Simulated thunderstorm in the towering cumulus stage 20 minutes into the simulation. Top frame is looking north at the vertical extent of the cloud. Bottom right is the top-down view of the thunderstorm and bottom left in the derived reflectivity. The cloud (in orange) is isosurfaced at 95% relative humidity.

Recall the input sounding (Fig. 10) used to initialize the simulation has westerly winds that increase with height. The drier westerly winds are ingested into the storm since storm propagation is slower than the mid and upper level winds. The drier winds act to evaporate the rain and cloud water in the storm. The evaporatively cooled air becomes more dense and falls to the surface and spreads out horizontally to form the cold pool. As the cold pool forms under the storm, low level air is forced upward into the updraft. The baroclinic region along the edge of the gust front is also a region where horizontal vorticity is tilted in to the vertical. This feature can be seen in a cross section through the storm along with the initial storm rotation starting to develop in Figure 13.

Figure 13. Cross section of potential vorticity from 975 mb to 250 mb through the thunderstorm at 15 minutes into the simulation. Two areas of positive values are noted, one at the surface and one near 850 mb.

The baroclinic generation of vertical vorticity can be easily seen near the surface in the PV contours as well as the beginning stages of storm rotation. This is seen by the positive PV values near 850 mb and 500 mb. Also noted in the cross section is the region denoted by the negative values in PV. As horizontal vortex lines are displaced into the vertical, a cyclonic rotation is seen associated with the updraft while an anticyclonic rotation is associated with downdraft. The calculated PV field corresponds to these features.

B. CELL SPLITTING

The original storm begins to undergo splitting between 30 and 45 minutes into the simulation. This split produces a left and right moving supercell seen in Figure 14. Right movers produce deep cyclonic circulations while left movers develop anticyclonic circulations due to increasing vorticity that is advected into the updraft (Bluestein 1993).

Since the left and right moving storms have different rotation, an appropriate response should be seen in the PV distribution and the PV derived fields in the regions around the two storms (Figure 15).

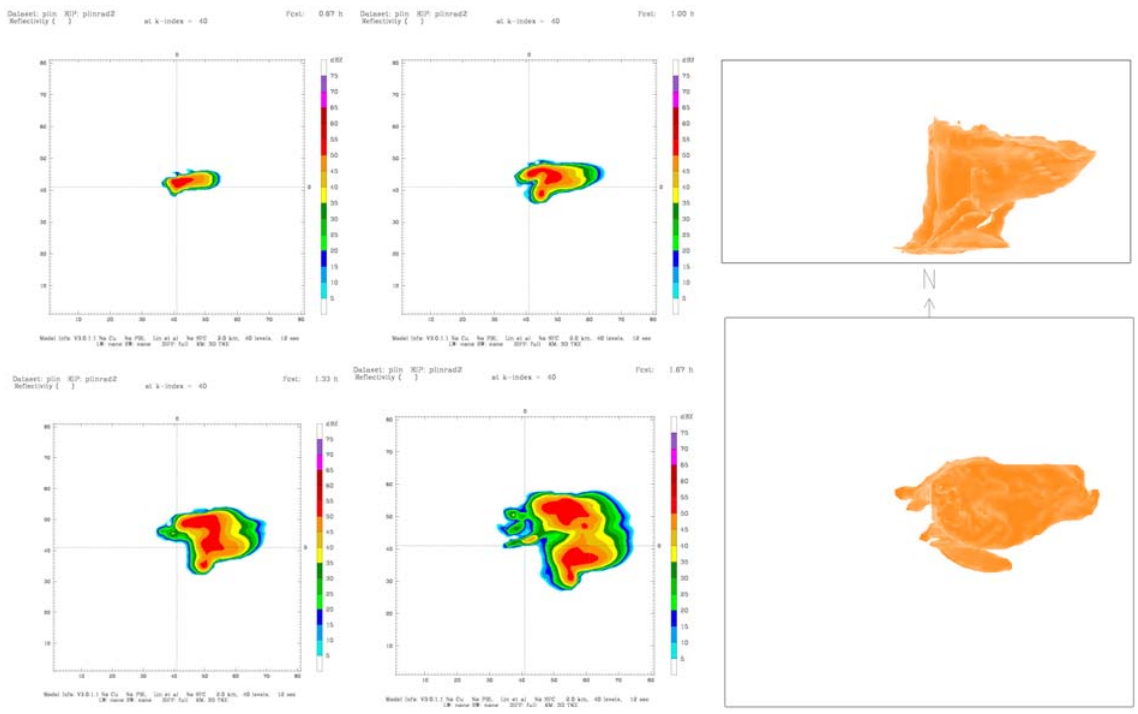

Figure 14. Model derived radar reflectivities showing the splitting supercells. Images taken every 20 minutes. Radar sections: Top left at 40 minutes, top center at 60 minutes, bottom left at 80 minutes and bottom center at 100 minutes. The right panels show the thunderstorm with relative humidity isosurfaced at 95% with the top right looking north and the bottom right looking top down at 50 minutes into the simulation.

The convection at one hour is located near the leading edge of the cold pool. The low level easterly winds have prevented the cold pool from running ahead of the thunderstorm and cutting off the supply of warm air from the updraft. This allowed for the sustainment of each of the supercells. Figure 15 shows the streamline analysis at one hour into the simulation. The original storm now identified as the left moving storm is still the dominant storm. The left moving cell has taken on anticyclonic flow as the right moving cell begins to develop along the edge of the cold pool.

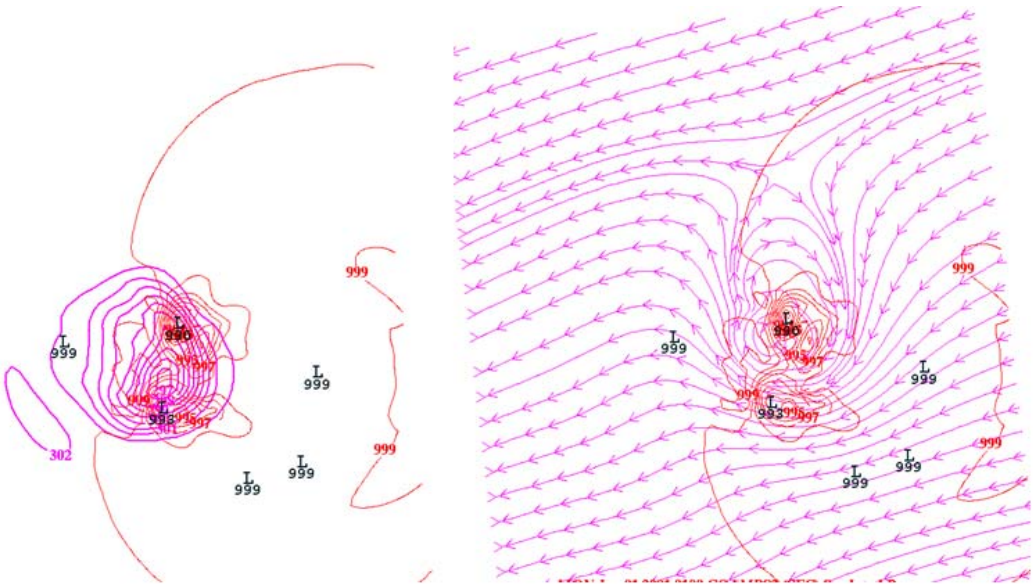

Figure 15. PV calculated fields at one hour into simulation and at 950 mb for (a) mean sea level pressure in red and potential temperature in purple and in (b) streamlines in purple.

Cross sections taken though both the left and right moving storms further support the underlying dynamics. Figure 16 shows both cells characterized by a nearly vertical shaft of PV associated with the updrafts in each of the storms. The anticyclonic updraft of the left mover is given by the negative values in PV while the cyclonic updraft in the right mover is represented by positive PV values. The lower levels beneath both thunderstorms are characterized by strong positive values of PV that signifies the baroclinic generation of vorticity up and over the cold pool into the storms' updrafts. Another feature to note in the right mover cross section is the area of negative PV values located in the lower levels on the western flank of the storm. These negative PV values are most likely a result of the cold pool left in the wake of the thunderstorm. The isentropes are bulging upward in the same manner as those in Thorpe (1985) for a negative surface potential anomaly.

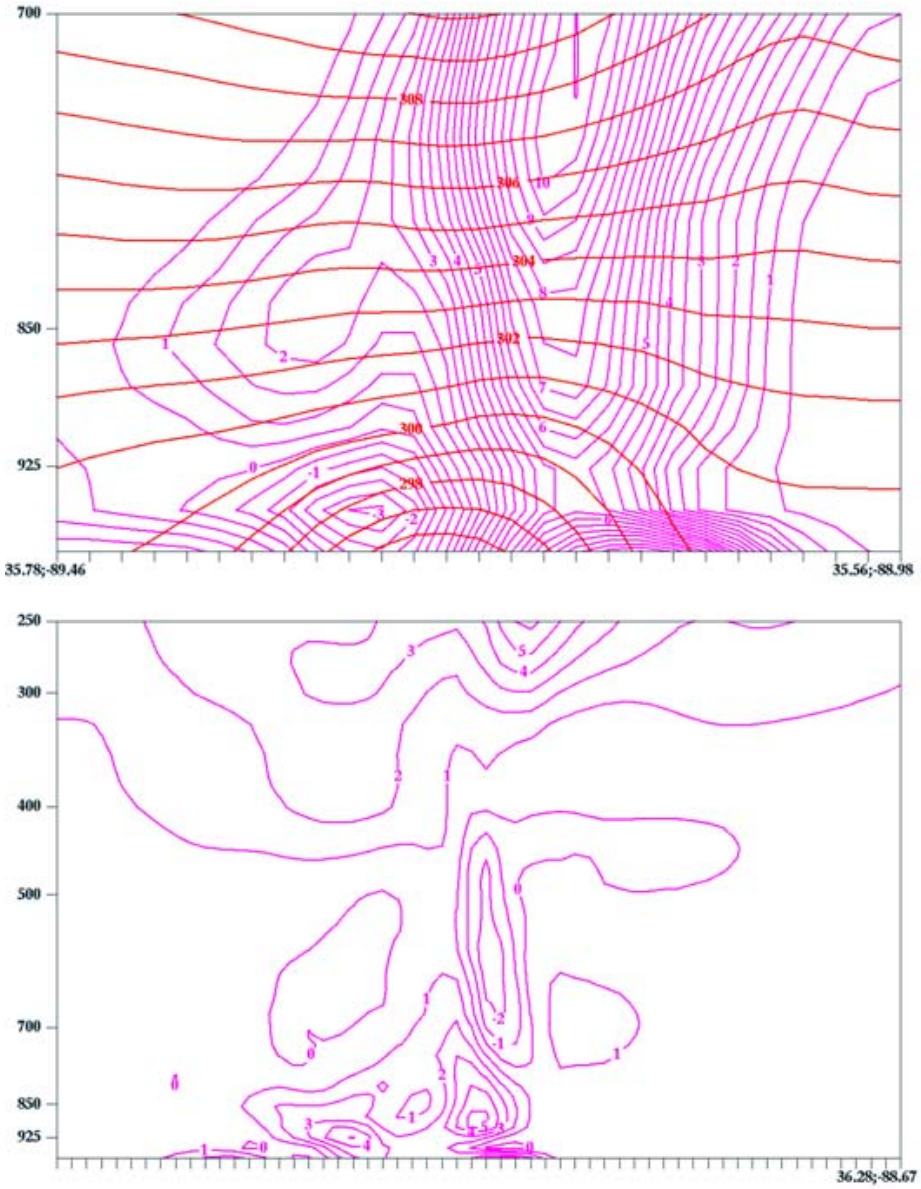

Figure 16. Cross sections take through the right mover (top) and left mover (bottom). The right mover is characterized by upward bulging isentropes (red) in the low level associated with the pool as well as negative PV values on the western section of the cold pool. Positive PV values correspond to a cyclonic updraft and large values of PV along the leading edge correspond to the generation of vertical vorticity. The left mover has the same features (isentropes not shown) with the exception of negative PV with the anticyclonic storm rotation.

The balanced flow based on the NLB PV inversion technique through the early stages of convective development and the beginning of storm splitting have so far been qualitatively accurate with other observational and other numerical studies of thunderstorms. These results seem promising at least for the beginning stages. It remains to be seen however, how well the NLB PV inversion will hold up as these cells intensify and the observed flow becomes more unbalanced.

C. SUPERCELL DEVELOPMENT

The right moving storm continues to evolve as it maintains a low level baroclinic vorticity contribution to its low level rotation. The right mover begins to evolve into more of the classic supercell as seen on radar. By 90 minutes into the simulation, the right mover has begun to develop a "v-notch" and the formation of a pendant or hook echo signature in the model derived radar reflectivities which suggest an intensification of the thunderstorm. Figure 17 shows the simulated supercell at two hours into the simulation.

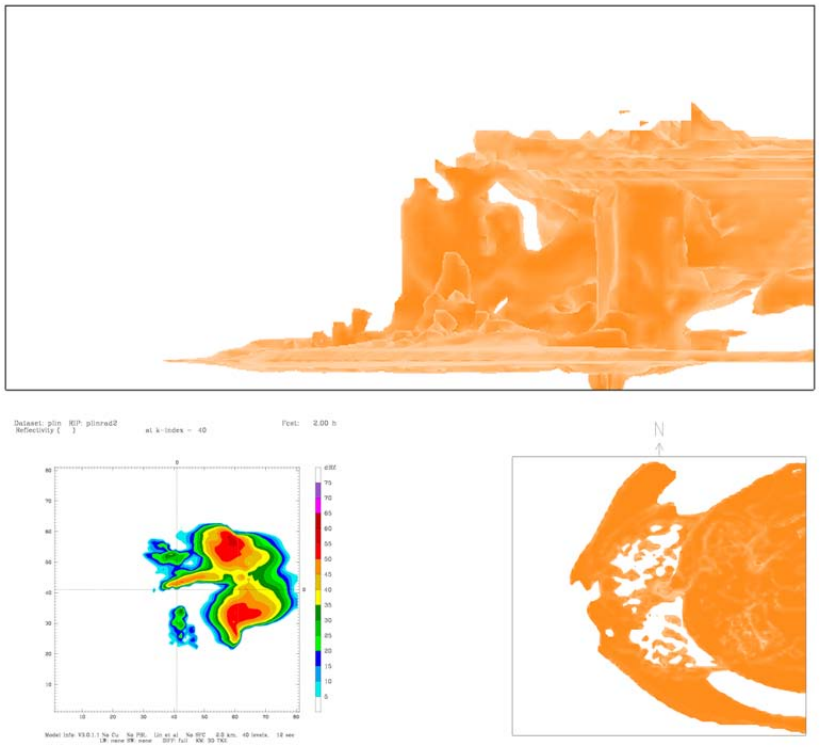

Figure 17. As in Figure 12, but at two hours into the supercell simulation

The intensifying supercell presents some problems for the PV inversion since we are using the NLB constraint. Atmospheric motions associated with thunderstorms are highly ageostrophic so the application of a balance constraint to retrieve an accurate estimate of the storm's wind field from the PV inversion might prove problematic.

Figure 18 shows the mean sea level pressure and wind field at two hours into the simulation. There are noticeable discrepancies associated with the balanced wind speeds in the vicinity of the two supercells. While the wind speeds are over-forecasted near the thunderstorms, especially the right mover, the flow pattern around each of the storms in correct. The right mover has cyclonic flow and the left mover has anticyclonic flow.

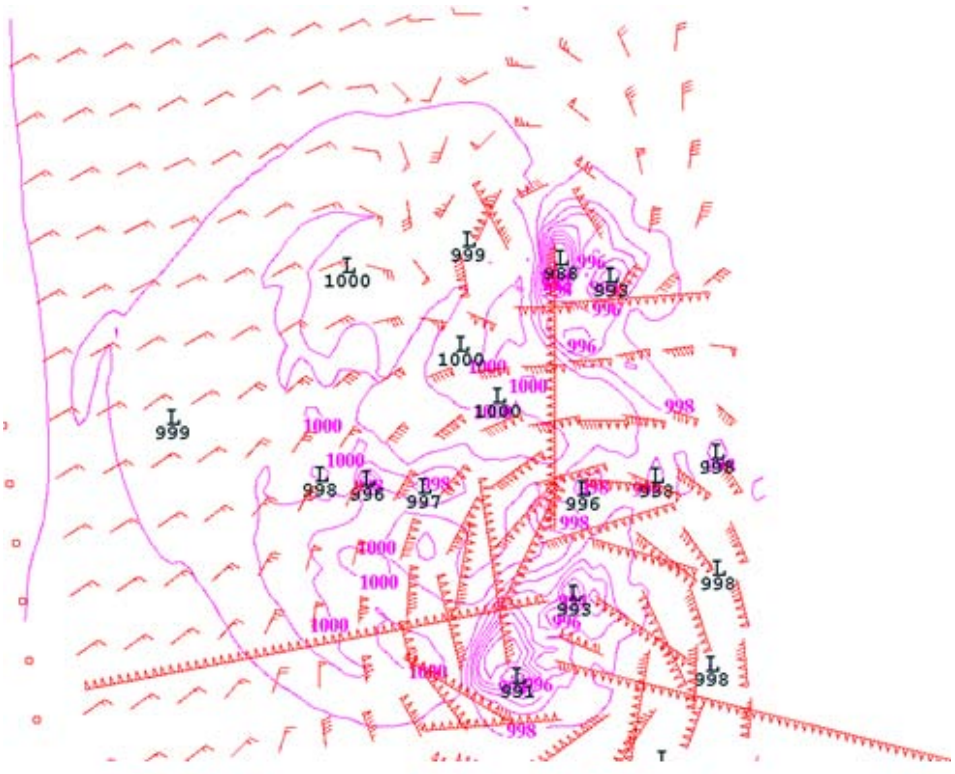

Figure 18. The balanced winds retrieved from the NLB PV inversion at two hours into the simulation with wind barbs at 950 mb.

Over-looking the gross errors from the balanced winds, the inversion process does identify the generation of new convection/splitting cell formation associated with the right moving supercell. Focusing on the right mover, the balanced streamlines (not

shown here) identify two cyclonic rotations associated with two low pressures and an anticyclonic rotation separating the updrafts.

To further understand the possible reason behind the over-forecasted wind speeds, Figure 19 shows the absolute vorticity and balanced streamfunction. High values of vorticity are seen around both thunderstorms. Focusing on the right moving supercell, there is a large value of low level vorticity associated with the low level cyclonic circulation. This value of absolute vorticity is orders of magnitude larger than normal for larger scale systems.

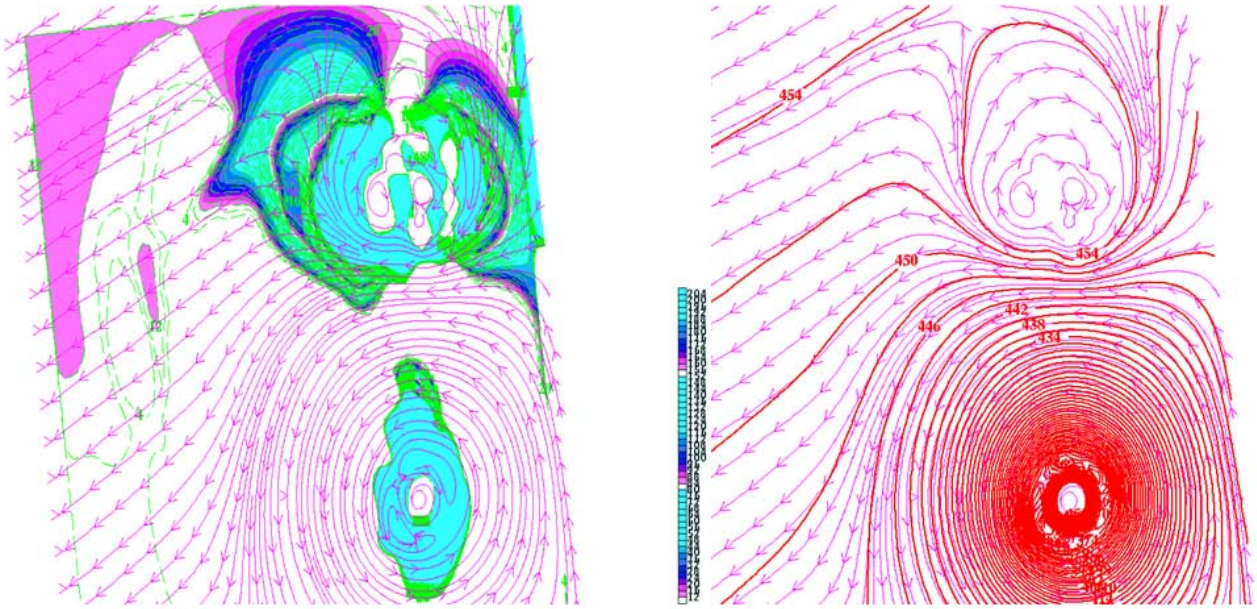

Figure 19. The absolute vorticity (right) and streamfunction (left) along with streamlines (purple) at 950 mb.

Recalling the Rossby/Ertel form of PV in Eq (1), gravity and the Coriolis are constants and the static stability around the right mover is not changing enough to generate this kind of change in the PV field. This leaves the relative vorticity as the likely source of the increase in PV. Figure 20 shows the three-dimensional evolution of the right mover beginning at 80 minutes into the simulation through two hours.

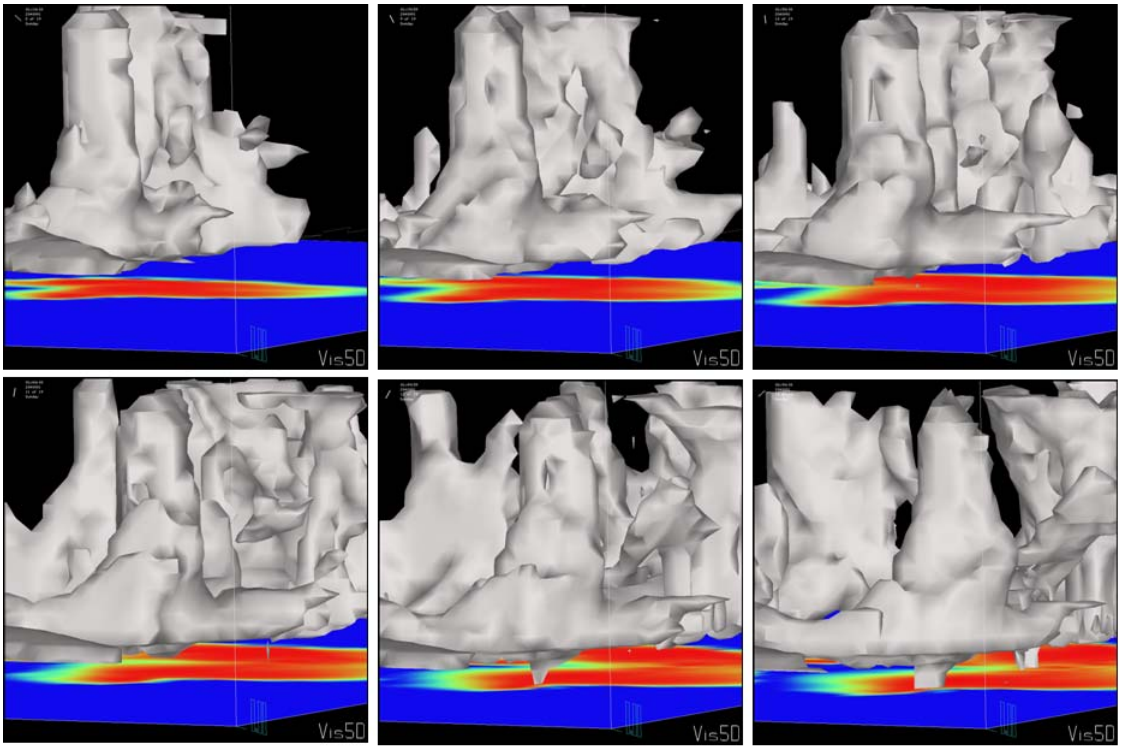

Figure 20. Time series of simulated tornadic development. Moving from left to right, series starts at 70 minuets in the simulation and ends at 120 minutes in the bottom right. Clouds (white) isosurfaced at 95% relative humidity with model derived reflectivity values on the bottom.

As the right mover evolves and intensifies along the leading edge of the cold pool, the low level rotation is constantly being fed from the low level baroclinic generation of vorticity. As the circulation becomes tighter and stronger during tornadogenesis, the derived balance wind field must see a response. The direct consequence to the dramatic increase in relative vorticity is the unproportional balanced wind field during this period of the simulation.

Overall, the qualitative ability of the NLB PV inversion to handle storm-scale dynamics was impressive. During the early parts of convective development the retrieved wind and mass fields closely resembled those observed in the simulation. The later stages of convection produced more of a problem since the highly ageostrophic nature of convection puts strain on most any balanced flow constraint.

V. CONCLUSIONS AND FUTURE RESEARCH

A. SUMMARY AND CONCLUSIONS

The goal of this study was to see if PV inversion that utilizes the NLB constraint could be successfully applied to meso- and even storm-scale dynamics. The results presented here show that there is a good qualitative agreement from the balanced flow to what is observed in the thunderstorms. This leads us to the ability to characterize storm-scale features in term of PV anomalies to diagnose thunderstorm dynamics.

Cyclonically (anticyclonically) rotating updrafts (downdrafts) or right (left) moving storms can be described in terms of a positive (negative) PV anomaly. The surface cold pool which also plays an important role in convective development is seen to possess both aspects of positive and negative PV anomalies. The leading edge of the cold pool is a region of baroclinic vorticity generation and thus a positive PV anomaly, while the trailing end resembles the cold dome described by Thorpe (1985) as a negative surface potential temperature anomaly. Even though the balanced flow was shown to be in qualitative agreement with the observed flow, more diagnostics are needed to verify the accuracy of this technique as it has been applied here.

B. FUTURE RESEARCH

The choice of the NLB constraint seems to be the biggest cause of error in the inversion technique. While the early time periods appear to show some accuracy, the later periods of the simulation have grossly over-forecasted winds due to the dramatic increase in low level relative vorticity at that time. The development of a cyclostrophic balance constraint would be beneficial for flows with large to infinite Rossby numbers (Davis and Weisman 1994).

Another aspect to consider follows the work of the Gold and Nielsen-Gammon (2008 four part series). The used PV inversion to link the convective parameters to the PV distribution based on the invertibility principle. By linking features like the cold pool to PV anomalies, the effects such a feature has on the convective environment might be better diagnosed.

While not related to the avenue of this research, multiple supercell simulations were conducted with various microphysics schemes. A large difference was noted among the various schemes used even though the model was initialized exactly the same each time. Since each of the microphysics schemes treats hydrometeors in slightly different way, the formation of certain storm features could be drastically different. This effect could be seen in the model generation of low level rotation. The mid level storm rotation acts to wrap hydrometeors (namely rain) around the updraft while the storm-relative wind push rain away from the updraft. The less rain available to wrap around the updraft, less evaporative cooling of air in the downdraft would produce a weaker cold pool and weaken the low level baroclinic generation of vorticity along the cold pool (Brooks et al. 1994a)

More diagnostics are also need to verify the accuracy of the inversion technique, solving for the omega equation to compare updraft strengths is one example. Given the good qualitative results shown here, it seems feasible that PV inversion can be applied to smaller scales than what it was initially created to do.

LIST OF REFERENCES

Bluestein, H.B., 1993: *Synoptic-Dynamic Meteorology in Midlatitudes. Vol II: Observations and Theory of Weather Systems*. Oxford University Press, 593 pp.

Brock, F.V., K.C. Crawford, R.L. Elliott, G.W. Cuperus, S.J. Stadler, H.L. Johnson, and M.D. Eilts, 1995: The Oklahoma Mesonet: A Technical overview. *J. Atmos. Oceanic Technol.*, **12**, 5–19.

Brooks, H.E., D.J. Stensrud, and J.V. Cortinas Jr., 1993: The use of mesoscale models to initiialize cloud-scale models for convective forecasting. Preprints, *14th Conf. on Weather Analysis and Forecasting*, Vienna, VA, Amer. Meteor. Soc., 301-304.

Brooks, H.E., C.A. Doswell, and J. Cooper, 1994: On the environments of tornadic and nontornadic mesocyclones. *Wea. Forecasting*, **9**, 606–618.

Brooks, H.E., C.A. Doswell, and R.B. Wilhelmson, 1994: The role of midtropospheric winds in the evolution and maintenance of low-level mesocyclones. *Mon. Wea. Rev.*, **122**, 126–136.

Bryan G.H., D. Ahijevych, C. Davis, S. Trier, and M. Weisman, 2005: Observations of cold pool properties in mesoscale convective systems during BAMEX. Preprints, *11th Conf. on Mesoscale Processes*, Albuquerque, NM, Amer. Meteor. Soc., JP5J.12. [Available online at http://ams.confex.com/ams/pdfpapers/96718.pdf] Accessed 03/2009.

Bunkers, M.J., B.A. Klimowski, J.W. Zeitler, R.L. Thompson, and M.L. Weisman, 2000: Predicting supercell motion using a new hodograph technique. *Wea. Forecasting*, **15**, 61–79.

Burgess, D.W., L.R. Lemon, 1991: Characteristics of mesocyclones detected during a NEXRAD test. Preprints, *25th Int. Conf. on Radar Meteorology*, Paris, France, Amer. Meteor. Soc., 39-42.

Byers, H.R., and R.R. Braham, 1948: Thunderstorm structure and circulation. *J. Atmos. Sci.*, **5**, 71–86.

Charney, J., 1955: The use of the primitive and balance equations. *Tellus*, **7**, 22-26.

Davies-Jones, R., 1984: Streamwise vorticity: The origin of updraft rotation in supercell storms. *J. Atmos. Sci.*, **41**, 2991–3006.

Davies-Jones, R., and H.E. Brooks, 1993: Mesocyclogenesis from a theoretical perspective. *The Tornado: Its Structure, Dynamics, Prediction and Hazards. Geophys. Monogr*. **49**, Amer. Geophys. Union, 104-114.

Davis, C.A., and K.A. Emanuel, 1991: Potential vorticity diagnostics of cyclogenesis. *Mon. Wea. Rev.*, **119**, 1929–1953.

Davis, C.A., E.D. Grell, and M. Shapiro, 1996: The Balanced dynamical nature of a rapidly intensifying oceanic cyclone. *Mon. Wea. Rev.*, **124**, 3–26.

Davis, C.A., and M.L. Weisman, 1994: Balanced dynamics of mesoscale vorticies produced in simulated convective systems. *J. Atmos. Sci.*, **51**, 2005-2030.

Dickinson, M.J., L.F. Bosart, W.E. Bracken, G.J. Hakim, D.M. Schultz, M.A. Bedrick, and K.R. Tyle, 1997: The March 1993 superstorm cyclogenesis: Incipient phase synoptic- and convective-scale flow interaction and model performance . *Mon. Wea. Rev.*, **125**, 3041–3072.

Doswell, C.A., 1987: The Distinction between large-scale and mesoscale contribution to severe convection: A case study example. *Wea. Forecasting*, **2**, 3–16.

Doswell, C.A., 2001: Severe convective storms – An overview. *Severe Convective Storms, Meteor. Mongr.*, No. 50, Amer. Meteor. Soc., 1-26.

Droegemeier, K.K., S.M. Lazarus, and R. Davies-Jones, 1993: The influence of helicity on numerically simulated convective storms. *Mon. Wea. Rev.*, **121**, 2005–2029.

Dudhia, J., 2006: WRF physics options. [Available online at www.dtcenter.org/events/wrf-nmm_tutorial06_summer/Presentations/NMM_Physics_Dudhia.pdf]. Accessed 03/2009.

Engerer, N.A., D.J. Stensrud, and M.C. Coniglio, 2008: Surface characteristics of observed cold pools. *Mon. Wea. Rev.*, **136**, 4839–4849.

Ertel, H., 1942: Ein neuer hudrodynamishcher wirbelsatz. *Met. Z.*, **59**, 271-281.

Gerard, A., C. Mead, S. Miller, R. Post, and P. Wolf, 1998: Surprise snow storm socks Louisiana, Mississippi, and Alabama. NOAA Tech. Attachment NWS SR/SSD 98-5.

Gold, D.A., and J.W. Nielsen-Gammon, 2008a: Potential vorticity diagnosis of the severe convective regime. Part I: Methodology. *Mon. Wea. Rev.*, **136**, 1565–1581.

Gold, D.A., and J.W. Nielse-Gammon, 2008b: Potential vorticity diagnosis of the severe convective regime. Part III: The Heston tornado outbreak. *Mon. Wea. Rev.*, **136**, 1593-1611.

Gold, D.A., and J.W. Nielsen-Gammon, 2008c: Potential vorticity diagnosis of the severe convective regime. Part IV: Comparison with modeling simulations of the Moore tornado outbreak. *Mon. Wea. Rev.*, **136**, 1612–1629.

Holton, J.R., 1992: *An Introduction to Dynamic Meteorology.* 3d ed. Academic Press, 511 pp.

Hoskins, B.J., M.E. McIntyre, and A.W. Robertson, 1985: On the use and significance of isentropic potential vorticity maps. *Quart. J. R. Met. Soc.,* **111**, 877-946.

Huo, Z., D.L. Zhang, and J.R. Gyakum, 1999: Interaction of potential vorticity anomalies in extratropical cyclogenesis. Part II: Sensitivity to initial perturbations. *Mon. Wea. Rev.*, **127**, 2563–2575.

Johns, R.H., and C.A. Doswell, 1992: Severe local storms forecasting. *Wea. Forecasting*, **7**, 588–612.

Johns, R.A., J.A. Hart, 1993: Differentiating between types of severe thunderstorm outbreaks: A preliminary investigation. Preprints. *17th Conf. on Severe Local Storms*, St. Louis, MO, Amer. Meteor. Soc., 46-50.

Johnson, R.H., B.E. Mapes, 2001: Mesoscale processes and severe convective weather. *Severe Convective Storms, Meteor. Mongr.,* No. 50, Amer. Meteor. Soc., 71-122.

Jukes, M., R.K. Smith, 2000: Convective destabilization by upper level troughs. *Quart. J. R. Met. Soc*., **126**, 111-123

Kleinschmidt, E., 1950a: Uber Aufbau und Entstehung von Zyklonen (1. Teil). *Met. Runds*., **3**, 1-6.

Kleinschmidt, E., 1950b: Uber Aufbau und Entstehung von Zyklonen (2. Teil). *Met. Runds*., **3**, 54-61.

Kleinschmidt, E., 1951: Uber Aufbau und Entstehung von Zyklonen (3. Teil). *Met. Runds*., 4, 89-96.

Laprise, R., 1992: The Euler Equations of Motion with Hydrostatic Pressure as an Independent Variable. *Mon. Wea. Rev.*, **120**, 197–207.

Lemon, L.R., and C.A. Doswell, 1979: Severe thunderstorm evolution and mesocyclone structure as related to tornadogenesis. *Mon. Wea. Rev.*, **107**, 1184–1197.

Maddox, R., L.R. Hoxit, and C.F. Chappell, 1980: A Study of tornadic thunderstorm interactions with thermal boundaries. *Mon. Wea. Rev.*, **108**, 322–336.

Markowski, P.M., E.N. Rasmussen, and J.M. Straka, 1998: The occurrence of tornadoes in supercells interacting with boundaries during VORTEX-95. *Wea. Forecasting*, **13**, 852–859.

Moller, A.R., C.A. Doswell, M.P. Foster, and G.R. Woodall, 1994: The operational recognition of supercell thunderstorm environments and storm structures. *Wea. Forecasting*, **9**, 327–347.

Morgan, M.C., and J.W. Nielsen-Gammon, 1998: Using tropopause maps to diagnose midlatitude weather systems. *Mon. Wea. Rev.*, **126**, 2555–2579.

Newton, C.W., and H.R. Newton, 1959: Dynamical interactions between large convective clouds and environment with vertical shear *J. Atmos. Sci.*, **16**, 483–496.

Nielsen-Gammon, J.W., and D.A. Gold, 2008a: Potential vorticity diagnosis in the quasigeostrophic and nonlinear balance systems. *J. Atmos. Sci.*, **65**, 172–188.

Nielsen-Gammon, J.W., and D.A. Gold, 2008b: Potential vorticity diagnosis of the severe convective regime. Part II: The impact of idealized PV anomalies. *Mon. Wea. Rev.*, **136**, 1582–1592.

Ooyama, K.V., 1990: A Thermodynamic Foundation for Modeling the Moist Atmosphere. *J. Atmos. Sci.*, **47**, 2580–2593. Laprise 1992.

Purdom, J.F., 1976: Some uses of high-resolution GOES imagery in the mesoscale forecasting of convection and its behavior. *Mon. Wea. Rev.*, **104**, 1474–1483.

Roebber, P.J., D.M. Schultz, and R. Romero, 2002: Synoptic regulation of the 3 May 1999 tornado outbreak. *Wea. Forecasting*, **17**, 399–429.

Rossby, C.G., 1940: Planetary flow patterns in the atmosphere. *Quart. J. R. Met. Soc.*, **66**, (Suppl) 68-87.

Rotunno, R., and J. Klemp, 1985: On the rotation and propagation of simulated supercell thunderstorms. *J. Atmos. Sci.*, **42**, 271–292.

Rotunno, R., J.B. Klemp, and M.L. Weisman, 1988: A theory for strong, long-lived dquall lines. *J. Atmos. Sci.*, **45**, 463–485.

Skamarock, W.C., J.B. Klemp, J. Dudhia, D. Gill, D.M. Barker, M.G. Duda, X. Huang, W. Wang and J.G. Powers, 2008: A Description of the Advanced Research WRF Version 3., NCAR Tech. Note NCAR/TN-475+STR, 113 pp.

Szeto, K.K., and H.R. Cho, 1994: A numerical investigation of squall lines. Part II: The mechanics of evolution. *J. Atmos. Sci.*, **51**, 425–433.

Thorpe, A., 1985: Diagnosis of balanced vortex structure using potential vorticity. *J. Atmos. Sci.*, **42**, 397–406.

Thorpe, A.J., M.J. Miller and M.W. Moncrieff, 1982: Two-dimensional convection in nonconstant shear: A model of midlatitude squall lines. *Quart. J. Roy. Meteor. Soc.*, **108**, 739-762.

Wakimoto, R.M., 1982: The life cycle of thunderstorm gust fronts as viewed with Doppler radar and rawinsonde data. *Mon. Wea. Rev.*, **110**, 1060–1082.

Wang, W., D. Barker, C. Bruyere, J. Duda, D. Gill, J. Michalakes, and S. Rizvi, 2008: WRF Version 3 Modeling System User's Guide. [Available online at http://www.mmm.ucar.edu/wrf/users/docs/user_guide_V3/]. Accessed 03/2009.

Weisman, M., and J. Klemp, 1982: The dependence of numerically simulated convective storms on vertical wind shear and buoyancy. *Mon. Wea. Rev.*, **110**, 504–520.

Weisman, M., and J. Klemp, 1986: Characteristics of isolated convective storms. *Mesoscale Meteorology and Forecasting*, P. Ray, Ed., Amer. Meteor. Soc., 331–358.

Wicker, L.J., and W.C. Skamarock, 2002: Time-Splitting Methods for Elastic Models Using Forward Time Schemes. *Mon. Wea. Rev.*, **130**, 2088–2097.

THIS PAGE INTENTIONALLY LEFT BLANK

INITIAL DISTRIBUTION LIST

1. Defense Technical Information Center
   Ft. Belvoir, VA

2. Dudley Knox Library
   Naval Postgraduate School
   Monterey, CA

3. Air Force Technical Library
   Air Force Combat Climatology Center
   Asheville, NC

4. Prof. Wendell Nuss
   Naval Postgraduate School
   Monterey, CA

5. Lt Col. Karl Pfeiffer
   Naval Postgraduate School
   Monterey, CA

6. Robert Davenport
   25th Operational Weather Squadron
   Tucson, AZ